NASA TECHNICAL TRANSLATION NASA TT F-13,455

THERMAL RADIATION FROM THE MOON AND THE PHYSICAL PROPERTIES OF ITS UPPER MANTLE

V. S. Troitskiy and T. V. Tikhonova

Translation of "Teplovoye islucheniye luny
i fizicheskiye svoystva yeyo verkhnego pokrova,"
Izvestiya vysshikh uchebnykh zavedeniy,
Radiofizika, Vol. 13, No. 9, 1970, pp. 1273-1311.

N71-16861
(ACCESSION NUMBER)
64
(PAGES)
(NASA CR OR TMX OR AD NUMBER)
(THRU)
GR
(CODE)
30
(CATEGORY)
FACILITY FORM 602

FEB 1971
RECEIVED
NASA STI FACILITY
INPUT BRANCH

NATIONAL AERONAUTICS AND SPACE ADMINISTRATION
WASHINGTON, D. C. 20546 JANUARY 1971

TABLE OF CONTENTS

		Page
I.	Introduction	1
II.	The Theory of the Thermal Regime on the Surface.	
	1. General Relationships	3
	2. Thermal Regime During Lunation. Homogeneous Model of the Surface Layer	4
	3. Surface Thermal Regime During Eclipse	10
	4. The Effect of Roughness of the Surface on its Thermal Regime	12
III.	The Theory of Natural Thermal Radiofrequency Radiation from the Moon.	
	1. Radiofrequency Radiation from the Moon When the Heating of Its Surface is Periodic	15
	2. The Spectrum of the Constant Component of the Integrated Radiofrequency Radiation from the Moon	19
	3. Radiofrequency Radiation From the Moon During Eclipse	21
IV.	The Emissivity of the Surface of the Moon in the Radiofrequency Region	
	1. Emissivity of a Smooth Surface	24
	2. Emissivity of a Rough Surface	25
	3. Emissivity of the Surface Layer of the Moon Nonhomogeneous in Depth	26
	4. Polarization of Radiofrequency Radiation from a Rough Surface	28
V.	Results of Measurements of Natural Radiation From the Moon	
	1. Results of Infrared Measurements	32
	2. A Method for Making Precise Measurements of Radiofrequency Radiation from the Moon (the "Artificial Moon" Method)	35
	3. Experimental Data on Radiofrequency Radiation from the Moon During Lunation and During Eclipse	36

Page

VI. Results of the Measurement of the Spectrum of the Reflection Coefficient 39

VII. Laboratory Investigations of Terrestrial Rocks 40

VIII. Interpretation of the Data on Natural and Reflected Radiation, and on the Structure and Properties of the Upper Mantle of the Moon 44

1. Quasi-Homogeneity of the Properties of the Material in Depth 44

2. The Thermal Parameter γ 45

3. The Parameter $\delta = l_e/l_T$ 46

4. Density of the Material of the Surface Layer of the Moon 47

5. Thermal Conductivity, k, and Depth of Penetration of Heat Wave l_T 49

6. Electromagnetic Properties of the Material: Depth of Penetration of the Electrical Wave l_e; Permittivity ε; and the Specific Tangent of the Angle of Loss $\tan(\Delta/\rho)$ 49

7. Chemical Composition of the Lunar Material 50

8. The Microstructure of the Material of the Upper Mantle of the Moon 52

9. Homogeneity of Surface Properties 52

10. General Model of the Structure of the Upper Layer of the Moon 53

IX. Conclusion 55

THERMAL RADIATION FROM THE MOON AND THE PHYSICAL PROPERTIES OF ITS UPPER MANTLE

V. S. Troitskiy and T. V. Tikhonova

ABSTRACT. Investigations made of the moon's natural emissions, and of the reflection of radio waves from its surface, are summarized by type. A modern model of the structure of the upper mantle of the moon, based on available experimental data, and on the methods developed to interpret these data, is presented.

I. INTRODUCTION

This survey is a critical generalization of Soviet and foreign research on /1274* the moon's natural emissions in the infrared and radiofrequency bands, with the inclusion of radar data and laboratory investigations of the electrical and thermal properties of the earth analogs for the material of the moon's upper mantle.[1]

Prior to 1927, the only sources of information on the physical conditions on the moon were optical observations that provided information only on the condition of material on the surface. In 1927-30, Pettit and Nicolson [1] made the first measurements of the moon's natural emissions in the infrared band during lunation and eclipse. These measurements made it possible to establish the temperature on the surface of the planet, to estimate the thermal conductivity of the lunar material, and to draw the first conclusions concerning the structure of the moon's material.

In 1946, measurements were made of the natural emission of radiofrequencies from the moon $\lambda = 1.25$ cm [2]. Since that time we have obtained a vast amount of experimental material on such emissions over a broad wave band. These investi-

---

1. The author, naturally, wishes to state that the survey expresses the point of view developed by associates in the Gor'kiy Scientific-Research Radiophysics Institute (NIRFI), where many of the theoretical and experimental investigations were made.

*Numbers in the margin indicate pagination in the foreign text.

gations, together with the data from radar and infrared measurements, obtained abroad for the most part, make it possible to draw a rather complete, inherently non-contradictory, picture of the physical conditions on the moon. Generalization of the results obtained prior to 1965 are contained in [3-5], and those prior to 1967 in [6]. The purpose of this survey is to summarize by type the investigations made of the moon's natural emissions, and of the reflection of radio waves from its surface, and to present a modern model of the structure of the upper mantle of the moon based on available experimental data and on the methods developed to interpret these data.

II. THE THEORY OF THE THERMAL REGIME ON THE SURFACE

1. General Relationships

The principal characteristics of radiofrequency emissions from the moon, since they are thermal, can be established by conditions prevailing for heating the moon's surface by solar radiation. The thermal regime for the lunar surface, and the temperature distribution in depth, can be described by thermal conductivity equations with the corresponding boundary and initial conditions

$$\frac{\partial}{\partial y}\left[k(y, T)\frac{\partial T}{\partial y}\right] = \rho(y)\, c(y, T)\frac{\partial T}{\partial t}. \tag{1}$$

In the event of a periodic thermal regime (lunation), the boundary conditions have the form

$$\left(k_s \frac{\partial T}{\partial y}\right)_{y=0} = \sigma(1 - R_{in})[T(0, t)]^4 + q - \begin{cases} S_0(1-R_1)\cos\psi\cos(\Omega t - \varphi) & \left(|\Omega t - \varphi| \leqslant \frac{\pi}{2}\right) \\ 0 & \left(\frac{\pi}{2} < (\Omega t - \varphi) < \frac{3\pi}{2}\right) \end{cases} \tag{2}$$

and, in the case of an aperiodic regime (eclipse) will have the form /1275

$$\left(k_s \frac{\partial T}{\partial y}\right)_{y=0} = \sigma(1 - R_{in})[T(0, t)]^4 + q - S_0(1 - R_1)\cos\psi\cos\varphi\, f(t). \tag{3}$$

In Eqs. (1 - 3), $\rho(y)$ is the density of the lunar material, c(y, T) is the specific heat, q is the density of the heat flow from the moon's interior, σ is the Stefan-Boltzmann constant, R_1 and R_{in} are the light and infrared albedo for the surface, respectively, S_0 is the solar constant, f(t) is a function of the change in the flux during eclipse, φ and ψ are the longitude and latitude of a surface element, respectively, the thermal regime of which is being considered, Ω is the frequency of lunation, $k(y, T) = k_0 + k_r$ is the total thermal conductivity, equal to the sum of the molecular, k_0, and radiative k_r, thermal conductivity, and $k_s = k_0 + k_{rs}$, k_{rs} is the radiative thermal conductivity of the surface.

As has been pointed out in [7], when radiative thermal conductivity is present in a solid, porous body transparent to infrared waves, the heat transport

equation and the boundary condition will contain different coefficients of radiative thermal conductivity. It is found that k_{rs} in the boundary condition is less by a factor of $2n^2/(1 - R_i)f(n)$ than is k_r in the differential equation, with n and R_i the index of refraction and the coefficient of reflection of the infrared waves in the body, respectively; $f(n) = n^2[1 - (1 - 1/n^2)^{3/2}]$. The initial conditions in the case of the computation for the lunation regime are arbitrary because a stabilized, induced, periodic solution is sought. In the case of eclipse, the initial conditions can be established by the temperature distribution prior to the beginning of the eclipse. Because eclipse occurs only during full moon, this temperature distribution will be obtained as the solution of the thermal conductivity equation for the lunation regime at time t = 0.

The problems involved in the investigation of the thermal regime during lunation and eclipse can be broken down into two types.

(1) Solution of Eq. (1) with the boundary conditions of Eq. (2), or of Eq. (3), when the solar energy flux S_0, or $S_0 f(t)$, can be considered as given. The solution of problems of this type cannot be obtained analytically; it can be computed on an electronic computer.

(2) Solution of Eq. (1) for a given surface temperature. Sunshine is periodic in nature during lunation, so the most convenient form for the assignment of the surface temperature is that of a function represented in the form of a Fourier series. The curve of the change in surface temperature during eclipse can be approximated quite well by four linear segments. The solution of problems of this type provides an analytical expression for the temperature distribution in depth, knowledge of which is needed in the computations for radiofrequency emissions from the moon.

2. Thermal Regime During Lunation. Homogeneous Model of the Surface Layer.

Some model of the structure of the upper layer must be adopted in order to compute the thermal regime for the surface. A homogeneous model in which the properties of the material do not change with depth, and which do not depend on temperature, was selected as a first approximation. It was found that in this case the surface temperature depended on but one parameter, $\gamma = (k\rho c)^{-1/2}$.

The problem of the first type for the homogeneous model of the structure of the upper layer was considered first by Wessilenk [8], and then in more

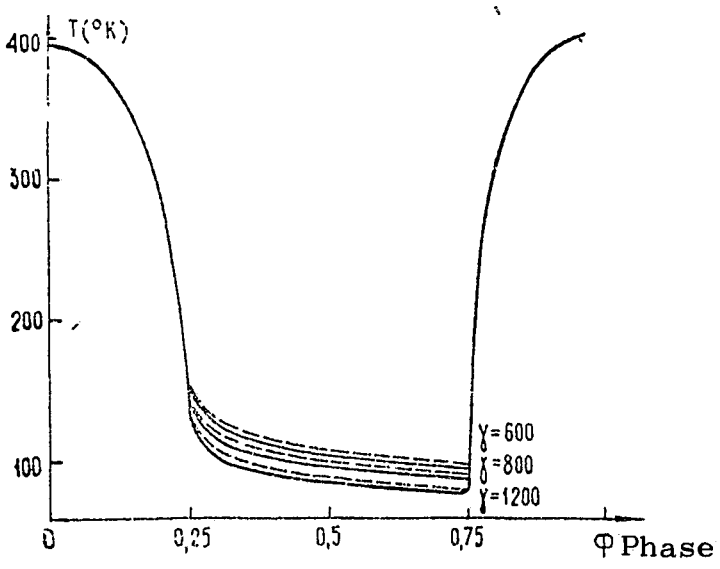

Figure 1. Change in the surface temperature in the center of the lunar disk in terms of the phase for parameter values γ = 600; 800; 1200. The solid curves are for the homogeneous model, without consideration having been given to the dependence of material properties on temperature. The dashed curves take this dependence into consideration.

detail, by Jaeger [9]. Jaeger solved Eq. (1), using the boundary condition of Eq. (2), by the numerical integration method, in order to find the change in surface temperature in the center of the lunar disk. /1276

References [10, 11] investigated the temperature regime on the lunar surface in more detail, using recent data on the magnitude of the solar constant. Figure 1 shows the surface temperature in the center of the lunar disk in terms of the phase angle (solid curves), obtained from the solutions of Eqs. (1) and (2) for various values of the parameter γ using an electronic computer.

The results of the surface temperature computations can be presented in the form

$$T(\varphi, \psi, t) = T_0(\psi) + \sum_{n=1}^{\infty} (-1)^{\alpha_n} T_n(\psi) \cos(n\Omega t - n\varphi - \varphi_n), \qquad (4)$$

where

φ_n is phase shift for the n^{th} harmonic of the change in the surface temperature in terms of the phase of the incident flux.

As has been shown in [10], the first five harmonics of $T_n(\psi)$ can be approximated quite well by the expressions

$$\begin{aligned} T_0(\psi) &= T_0(0)\cos^{0,25}\psi, & T_3(\psi) &= T_3(0)\cos^{0,44}\psi, \\ T_1(\psi) &= T_1(0)\cos^{0,33}\psi, & T_4(\psi) &= T_4(0)\cos^{0,3}\psi, \\ T_2(\psi) &= T_2(0)\cos^{0,27}\psi, \end{aligned} \qquad (5)$$

and the sign of these harmonics can be established by the exponent $\alpha_n = (n - 1)(n - 2)/2$.

Reference [72] solved the problem of the second type analytically for this same homogeneous model of the structure of the upper layer. The solution of Eq. (1), using boundary condition of Eq. (4), results in the following expression for temperature distribution in depth at any point on the lunar surface with

coordinates (φ, ψ)

$$T(y, \varphi, \psi, t) = T_0(\psi) + \sum_{n=1}^{\infty} (-1)^{\alpha_n} T_n(\psi) \exp\left(-y\sqrt{\frac{n\Omega\rho c}{2k}}\right) \times \cos\left(n\Omega t - n\varphi - \varphi_n - y\sqrt{\frac{n\Omega\rho c}{2k}}\right). \quad (6)$$

The temperature at any depth is the sum of a constant component and a variable one, formed by the sum of the harmonics with periods that are multiples of the lunation period ($\tau = 2\pi/\Omega = 29.5$ earth days). Each harmonic attenuates with depth, so that at depth $l_{Tn} = \sqrt{2k/n\Omega\rho c}$, the amplitude of the variation in temperature will be reduced by a factor of e, as compared with the surface value. This magnitude has been designated the temperature wave penetration depth. It characterizes the thickness of the surface layer heated by the sun in the course of a lunar day. There is practically no temperature variation at a depth three to four times that of l_T. /1277

A homogeneous model with a thermal conductivity and a specific heat dependent on temperature was considered in the second approximation. As is known, the thermal conductivity of porous bodies depends on temperature because of the radiative transport of heat through the pores. Radiative transport in a "lunar" temperature interval is accomplished by radiation on infrared waves, the lengths of which corresponds to the Planckian maximum $\lambda = 0.38/T \simeq 10$ to 30 microns. For a porous body, one in which the effective size of the pores is equal to l_n, and the material of which is not transparent to infrared waves, the magnitude of the radiative thermal conductivity, k_r, equals

$$k_{rn} = \frac{R_{in}}{2 - R_{in}} 4\sigma l_n T^3. \quad (7)$$

If the infrared waves penetrate the material, $k_r = (16/3)\sigma\varepsilon_n \bar{l}_v T^3$, where $\bar{l}_v$ is the Rosseland mean depth of penetration of the infrared radiation into the material, and ε_n is the permittivity of the material in the infrared band.

Computations show that for the relationship $\bar{l}_v = \alpha\lambda$ (which follows from the radio measurements and from the theory of nonresonant absorption of waves in a material) the magnitude $\bar{l}_v = 0.365\ \alpha/T$. From whence [13]

$$k_r = 2\varepsilon_{in} a \sigma T^2. \quad (8)$$

Total thermal conductivity is equal to the sum of the molecular and radiative thermal conductivity.

Jaeger made the first analysis of the moon's thermal regime with radiative thermal conductivity taken into consideration [9], but the computation brought no significant changes to the temperature in terms of phase.

Ingrao, Young, and Linsky [14] cite the results of the computations they made of the moon's surface temperature during lunation and eclipse for a homogeneous and for a double-layer model with the temperature dependence of thermal conductivity taken into consideration (specific heat was assumed constant). This same reference, [14], also contains the computations for the Muncey model [15], in which the dependence of the specific heat, and of the thermal conductivity, on the temperature was assumed to be linear. It was found that the nature of the drop in the temperature during sunset is satisfied by the Muncey model, as well as by the model with radiative thermal conductivity of the form $k_r = BT^3$. $T = 350°$ was obtained from the experiment in the first case when $\gamma = 400$ to 450, and in the second case when $\gamma = 600$.

Too, the authors of [14] note there are certain differences in the temperature distribution in depth, and that these differences are within a few centimeters of each other for two models indicated. Hence, there can be a difference in radiofrequency emissions in the millimeter wave band.

However, as the evaluations show, this difference is very slight, and cannot be detected in experiments yielding radiation phase behavior because these measurements are not accurate enough.

Reference [11] provides a detailed review of the question of the effect /1278
of the temperature dependence of the specific heat, and of the thermal conductivity, on the thermal regime and on the spectrum of radiofrequency emissions from the moon. Eq. (1), with the Eq. (2) boundary condition, was solved on an electronic computer assuming that the dependence of the specific heat on the temperature for the material of the moon's upper mantle was the same as it is for earth rocks, and further assuming that thermal conductivity does not depend on temperature. The computations reveal that taking the temperature dependence for the specific heat into consideration results in a somewhat deeper cooling of the moon's surface in the absence of sunshine.

Reference [11] further used the perturbation method to obtain an analytical solution of Eq. (1), using the Eq. (4) boundary condition for the case when the specific heat is c = constant, and the thermal conductivity is $k = k_0(1 + B_n T^n)$, where n = 1, 2, 3, and $B_n T^n < 1$ over the entire interval of lunar temperatures. The expression for the temperature distribution in depth for the center of the lunar disk in this case is in the form

$$T(y, t) = T_0 + \frac{n}{4} B_n T_0^{n-1} T_1^2 (1 - e^{-2\beta y}) + T_1 e^{-\beta y} \times$$
$$\times \cos(\Omega t - \varphi - \beta y)\left(1 + \frac{\beta B_n T_0^{n-1}}{2} y\right). \tag{9}$$

What follows from Eq. (9) is that the temperature dependence of the thermal conductivity (something that was pointed out for the first time in [33]) leads to an increase in the constant component of the temperature in depth, thanks to the unique effect of the detection of a temperature wave propagated in a nonlinear medium.

The electronic computer was used to obtain a precise solution of Eq. (1), using the Eq. (3) boundary condition for the center of the lunar disk [11] when the specific heat and the thermal conductivity depend on the temperature in the following manner, in order to evaluate the accuracy of the approximate analytical solution of Eq. (9)

$$c = c_n T, \qquad k = k_0(1 + B_n T^n).$$

The concordance between the precise solution and the approximate one is good.

Figure 1 shows the temperature at the center of the disk in terms of the local phase (the dashed curves) for different γ and $BT^3 = 0.5$. A comparison of these curves with the corresponding curves when the properties of the material do not depend on temperature (the solid curves) shows that giving consideration to the effect of the temperature dependencies of the specific heat and of the thermal conductivity results in no significant changes taking place in the surface temperature that will detract from the overall accuracy of the analysis and of the experiment.

If we are to evaluate the contribution of radiative transport, we must find phenomena that have very definite contributions to make to the dependence of

the thermal conductivity on the temperature. There is one such phenomenon, as has been found. As will be seen from Eq. (9), the constant component of the true temperature will increase with depth in accordance with the law

$$T_0(y) = T_0 + \Delta T_{\max}(1 - e^{-2y/l_T}), \tag{10}$$

where

ΔT_{max} depends on γ and on the magnitude of k_r.

An increase in the temperature with depth will result in an increase in the constant component of the radiofrequency emissions from the moon because of the increase in the wavelength. What follows from the computations is that the constant component of the brightness temperature of the radiofrequency emissions depends on the wavelength in accordance with the law [11]

$$T_{e0} \simeq T_0 + \Delta T_{max} \frac{2\delta}{1 + 2\delta}. \tag{11}$$

As will be shown in what follows, $\delta = 2.3\lambda$ for the moon. What this means is /1279 that on wavelengths of the order of 2 to 3 centimeters the constant component practically reaches its maximum $T_{eO} = T_O + \Delta T_{max}$. Thus, by measuring the temperature on the surface (on infrared waves) and in the depth (on waves with $\lambda \simeq$ (2 to 3) cm) we can find the rise in temperature ΔT_{max} and establish k_r/k_O.

The "artificial moon" method has made it possible to make accurate measurements of radiofrequency temperature. Reference [13] has shown that the significant difference between the infrared and radiofrequency measurements of the constant components of from 10° to 15° can be explained by the effect under consideration. When this was compared with the theory, it was found that if the moon material cannot be penetrated by infrared waves and has $\gamma \simeq 800$ kcal^{-1}-cm^2-sec$^{1/2}$-degree, the relative percentage of radiative transport through the pores when T = 300°K equals $k_{rn}(300)/k_O = 0.25$. If the material can be penetrated, $k_r(300)/k_O = 0.4$. Analogous numerical computations were made in [129].

References [9, 72], in addition to the homogeneous model, took up a two-layer model of the surface layer, in accordance with which the surface of the moon was represented as consisting of silicate rock with a low value for the thermal parameter, $\gamma \simeq 100$, and covered with a thin layer of dust for which

γ = 1000. However, as further investigations of radiofrequency emissions from the moon revealed, its surface layer has a quasihomogeneous structure in depth, so a sharply heterogeneous model should be rejected as not corresponding to the experimental data [16].

3. Surface Thermal Regime During Eclipse.

Jaeger [9] was the first to make a numerical computation of the moon's surface temperature. The Eq. (3) boundary condition was used with Eq. (1), and the solution was arrived at by assuming that the properties of the material remain unchanged with depth, and do not depend on the temperature. Reference [11] contains the computation made for the thermal regime of a surface element in the center of the lunar disk for the conditions that existed during the 1963 eclipse. The dependence of specific heat on temperature was considered in the form $c = c_0 T$, and the dependence of thermal conductivity on temperature was considered in the form $k = k_0(1 + BT^3)$.

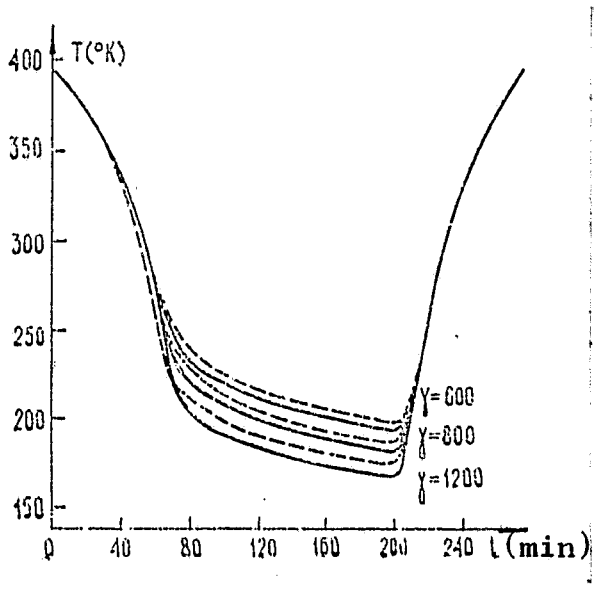

Figure 2. Change in the temperature of the surface in the center of the lunar disk during eclipse when γ = 600; 800; 1200. The solid curves do not take into consideration the dependence of the properties of the material on temperature; the dashed curves do take this dependence into consideration.

Figure 2 shows the change that takes place in the surface temperature during an eclipse when $BT^3 = 0.5$ (the dashed curves). These results were obtained by solving Eq. (1) and using the Eq. (3) boundary condition. (The solid curves are for the case when properties of the material do not depend on the temperature). /1280

Computations [9, 11] have shown that the presence of the c(T) and k(T) relationships for the lunar material have little effect on the thermal regime on the lunar surface, whether during lunation, or eclipse. This is the basis for the assumption that c = constant and k = constant when determining the surface temperature distribution over the visible disk of the moon [17] for four times during eclipse. The estimates have it that the surface temperature regime is completely restored, for all practical purposes, two hours after termination of the eclipse.

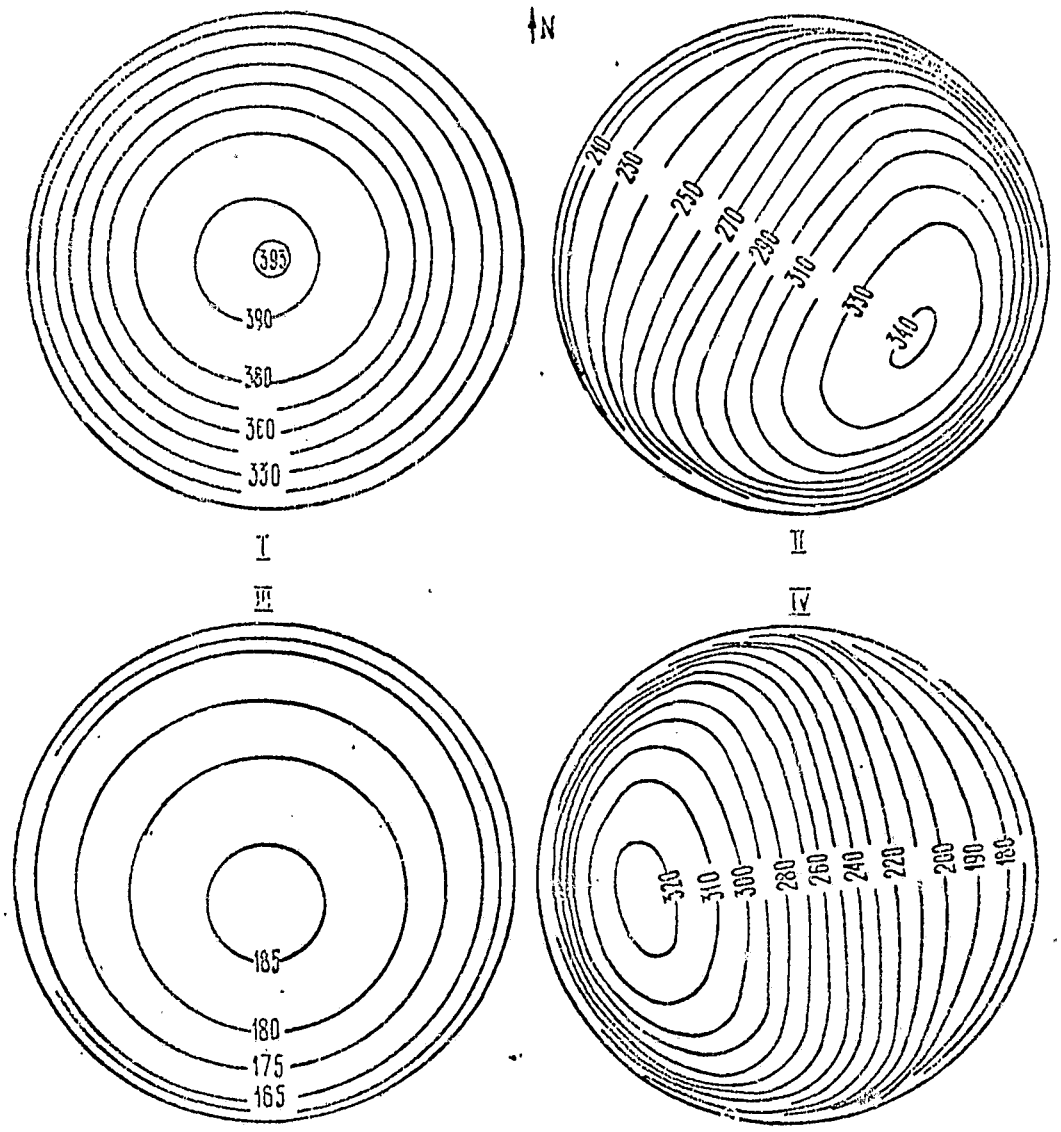

Figure 3. Temperature distribution over the visible disk of the moon for eclipse times 0, 100, 190, and 280 minutes.

Knowledge of temperature distribution in depth, T(y, t), is needed in order to develop a theory for radiofrequency emission during eclipse. References [18, 19] contain an analytical solution of the problem concerned with the moon's thermal regime during the period of eclipse. However, the solution of the thermal conductivity equation contained in [18] failed to take into consideration the initial temperature distribution T(y, 0). The problem, as solved in [19], assumed that the upper mantle was property homogeneous to a depth at which temperature variations during eclipse could still be found. A further assumption was that the properties of the material did not depend on temperature. The /1281 temperature of a surface element was considered as known at any moment in time

during the eclipse. In fact, the curve for surface temperature change during eclipse is known from a number of measurements (see [20], for example). This curve can be approximated quite well by four linear segments contained between characteristic moments of the eclipse, t_k

$$T(0, t) = T_k + \alpha_k(t - t_k), \quad \alpha_k = \frac{T_{k+1} - T_k}{t_{k+1} - t_k}, \quad \alpha_4 = 0$$
$$(k = 1, 2, 3, 4).$$

Here

t_1 is the time of beginning of the penumbral phase of the eclipse;

t_2 is the beginning of the umbral phase;

t_3 is the end of the umbral, and beginning of the penumbral phase;

t_4 is the end of the penumbral phase;

T_k is the surface temperature corresponding to time t_k.

The Eq. (6) temperature distribution, obtained from the solution of the thermal problem during lunation for the center of the disk ($\psi = 0$, $\varphi = 0$) and time $t = 0$ (full moon), is used as the initial condition.

4. The Effect of Roughness of the Surface on its Thermal Regime.

What follows from a theoretical analysis of the thermal regime on the lunar surface is that the temperature distribution along the smooth disk of a fully illuminated moon can be described by the law

$$T = T_0 \cos^{1/4}\psi. \tag{12}$$

However, the measurement results obtained by Pettit and Nicolson [1] were approximated quite well by an expression of the type

$$T = T_0 \cos^{1/6}\psi. \tag{13}$$

The authors explained the difference between Eqs. (12) and (13) by surface roughness.

Recent measurements made of the temperature distribution along an illuminated disk, carried out with high resolution during lunation in the far infrared and visible regions [21], yielded analogous results. These results made it

possible to compile an isotherm map showing that the temperature of a surface element depends on the sun's altitude, as well as on the angle of observation. These measurements confirmed the fact that the surface temperature distribution has the form of Eq. (13). Moreover, they confirmed the anomalies in the change in the temperature of the subsolar point. When the subsolar point moves to the edge of the disk, its temperature drops. Surface roughness evidently is the chief contributor to these effects. The literature on the subject considers two types of relief in this regard; small-scale nonuniformities, those from a millimeter to several centimeters, and large-scale irregularities of the order of a meter and more.

A model of a wavy surface was used in reference [22] to explain the anomolies in the change in the temperature of the subpolar point. It was shown that if the dimensions of the irregularity are of the order of millimeters and centimeters, and if incidence of the solar rays is normal, the temperature of this surface will be somewhat lower to the observer looking at the surface at some angle than will be the temperature of a flat surface made of the same material. Reference [23] explains this same effect with the help of spherical, more compact craters with centimeter dimensions.

The anomalies in the distribution of brightness over the disk of the moon are explained by large-scale nonuniformities. What usually is considered is a /1282 model in which fluctuations in height are distributed in accordance with a normal law, with the dimensions of the nonuniformities along the horizontal described by an exponential type autocorrelation function [24, 25]. A comparison between the theoretical computations made by Smith [25], and the experimental results obtained by Ingrao, Young, and Linsky [26], as well as by Saary and Shorthill [21], provides a means for estimating the magnitude of the mean square slope of the surface. This magnitude turns out to be 20°. Attempts to use this same analysis to explain the anomalies in the brightness of the subsolar point result in a greatly increased value for the mean square slope (60 to 70°), and this casts doubt on the assumptions on which the analysis is based.

Another fact that evidently can be of assistance in explaining these phenomena, and one that is discussed in the literature on the subject, is the pre-

sence of bed rocks on the moon's surface [27]. Reference [28] made quantitative estimates based on the assumption that the rock blocks consisted of basalt and were in the form of cubes. The general conclusion arrived at in [28] is that the effect of rocks at the center of the lunar disk at the infrared temperature is slight when observations are made from the earth. According to the author of [28], the effect of rocks measuring from a meter to several tens of meters can prove to be substantial when measurements are made from spacecraft because the sides turned toward the spacecraft and illuminated by the sun as it sets and rises can radiate over ten times more energy than can the rest of the surface.

III. THE THEORY OF NATURAL THERMAL RADIOFREQUENCY RADIATION FROM THE MOON

1. Radiofrequency Radiation from the Moon When the Heating of Its Surface is Periodic

Natural radiation from a medium can be described by the equation for the transfer of radiant energy. This equation can be simplified in the case of a dense material (such as that of the moon's surface layer), because the principle of local thermodynamic equilibrium can be used. Further simplification results from the fact that the thickness of the layer responsible for the radiation is much less than the radius of the planet, so can be considered as a plane problem. With everything that has been said thus far taken into consideration, the equation of radiation transfer on frequency v is in the form

$$\cos\vartheta \frac{d}{d\tau}\left(\frac{I_\nu}{n^2}\right) = -\frac{I_\nu}{n^2} + \frac{B_\nu}{n^2}; \tag{14}$$

$$B_\nu = \mu \int I_\nu f(r) \frac{d\omega}{4\pi} + (1 - \mu) n^2 B_{\nu_0}. \tag{15}$$

Here

$\tau = \int_0^1 \alpha_\nu \, dy$ is the optical thickness;

α_ν is the attenuation factor, equal to the sum of the true absorption factor, $(\varkappa)$;

$(\mu\alpha_\nu)$, μ the scattering factor, is a coefficient characterizing the ratio of the scattered power to the total amount absorbed;

n is the index of refraction for the waves in the medium;

f(r) is the scattering indicatrix;

ϑ is the angle between the vertical and the direction of radiation;

r is the angle between the direction of radiation incident to the elementary volume, and the direction of the radiation scattered by this volume;

B_{ν_0} is a function of the radiation from the medium.

In this case this is a Planck function for the flow of radiation from the medium in a vacuum.

If the medium is sufficiently homogeneous in depth in terms of its thermal and electrical properties, the solution of the transfer equation can be pre- /1283 sented in the form

$$I_\nu = (1 - R) \int_0^\infty B_\nu e^{-\tau \sec \vartheta} \sec \vartheta \, d\tau, \tag{16}$$

where

R is the coefficient of reflection of the radiation from the interface.

If the interface is smooth enough Fresnel formulas are correct for R. If the interface is very rough, R must be understood to be the albedo for the surface. If the medium is essentially inhomogeneous (for the given wavelength) Eq. (16) is complicated [29] because now the magnitude of R will depend on the optical depth τ and will have to be found by using Riccati differential equations [30]. Therefore, the coefficient of transmission of the radiation through the surface (1 - R) must be carried under the integral. The function of B_ν in Eq. (16) is an unknown function, found as the solution of Eq. (15).

All theories concerned with radiofrequency radiations from the moon up to this point were based on the assumption that $\mu = 0$ for radio waves. This is an accurate enough assumption, apparently, for waves longer than a millimeter. Scattering in the lunar material can prove to be substantial for waves shorter than millimeters. Thus, if $\mu = 0$, then $\alpha_\nu = \varkappa$, and $B_\nu = n^2 B_{\nu_0}$ is a known function, and the solution for the radiofrequency region, that is, when $h_\nu \ll kT$, is greatly simplified [12, 72]

$$T_e(0, l, \varphi, \psi) = [1 - R(\varphi, \psi)] \int_0^\infty T(y, \varphi, \psi, t) \varkappa \sec \vartheta' e \exp(-\varkappa y \sec \vartheta') dy, \tag{17}$$

where

T_e is the effective temperature of the radiation from an element of the surface with coordinates φ and ψ;

ϑ' is the angle at which the radiation strikes the interface from below;

$T(y, \varphi, \psi, t)$ is the true temperature of the moon material at depth y at time t, obtained above in the form of Eq. (6) as the solution of the thermal conductivity equation, Eq. (1), using the Eq. (4) boundary condition.

After this temperature distribution in depth is substituted in Eq. (17),

the result is the following expression for the effective temperature of an element of the surface [2]

$$T_e(\varphi, \psi, t) = [1 - R(\varphi, \psi)]\left\{T_0(\psi) + \sum_{n=1}^{\infty}(-1)^n \times \right.$$
$$\left. \times \frac{T_n(\psi)}{\sqrt{1 + 2\delta_n \cos\vartheta' + 2\delta_n^2 \cos^2\vartheta'}} \cos[n\Omega t - n\varphi - \varphi_n - \xi_n(\varphi, \psi)]\right\}, \quad (18)$$

where

$\delta = \sqrt{n\Omega\rho c'/2k}/\varkappa$ is the ratio of the depth of penetration of an electromagnetic wave $l_e = 1/\varkappa$ to the depth of penetration of the n^{th} harmonic of a thermal wave l_{nT}.

When the values for the tangent of the angle of losses are sufficiently small, the absorption factor equals $\varkappa = 4\pi\sigma'/c'\sqrt{\varepsilon}$, where σ' is the conductivity, and c' is the speed of light. The expression for δ then will take the form

$$\delta = \frac{c\gamma\lambda}{2\pi b\sqrt{\varepsilon}}\sqrt{\frac{\Omega}{2}},$$

where

$b = \tan\Delta/\rho$ is the specific tangent of the angle of losses;

$\xi_n = \arctan[\delta_n \cos\vartheta'/(1 + \delta_n \cos\vartheta')]$ is the phase shift for the n^{th} harmonic of the effective temperature with respect to the phase of the temperature of the surface.

The reception of integral radiofrequency radiation has been accomplished /1284 during experimental research on the moon when the width of the receiving antenna pattern at the 0.5 power level has been greater than the angular dimensions of the moon. Therefore, in order to obtain a correct interpretation of the results obtained from the measurements, one must compare them with the expression for integral radiation from the moon, obtained as a result of a precise solution. The theory of integral radiofrequency radiation is presented in [31] on the assumption of homogeneity of the properties of the moon's upper mantle.

According to [12], the averaged effective disk temperature equals

$$\overline{T}_e = \frac{1}{\pi} \int_{-\pi/2}^{+\pi/2} \int_{-\pi/2}^{+\pi/2} [1 - R(\varphi, \psi)]\, T_e(\varphi, \psi, t) \cos^2 \psi \cos \varphi \, d\varphi \, d\psi. \tag{19}$$

Since it is the central portions of the disk that make the principal contribution to the radiation, it is desirable to express the mean radiotemperature of the disk in terms of the radiation from the center of the disk, introducing the corresponding conversion factors. The result is the following expression for the effective temperature of the integrated radiofrequency radiation

$$\overline{T}_e = (1 - R_\perp)\, \beta_0\, T_0(0) + (1 - R_\perp) \sum_{n=1}^{\infty} (-1)^{\alpha_n} \frac{T_n(0)\, \beta_n}{\sqrt{1 + 2\delta_n + 2\delta_n^2}} \times \tag{20}$$
$$\times \cos(n\Omega t - \varphi_n - \xi_n + \Delta\xi_n),$$

where

β_0 and β_n are the corresponding averaging factors;

$\Delta\xi_n$ is the additional phase shift occurring during the averaging.

The magnitudes β_0, β_n and $\Delta\xi_n$ can be expressed in an extremely complicated manner in terms of the integrals that depend on ϵ and δ for the lunar surface. Their computations were made on an electronic computer for a wide range of changes in ϵ and δ. Figure 4 shows β_0 in terms of ϵ. Figure 5 and 6 show β_1 and β_2 in terms of δ_1 for various values of ϵ. Figure 7 is the additional phase shift, $\Delta\xi_1$, for the first harmonic in terms of δ_1. The maximum magnitude of $\Delta\xi_1$ is not in excess of -5°, even when there is a change in ϵ over broad limits. There is no such phase shift for the second harmonic of the integrated radiation, practically speaking.

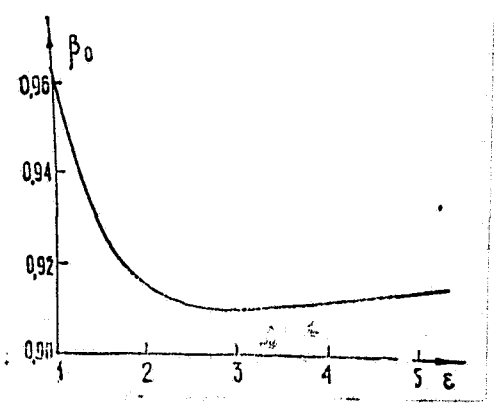

Figure 4.

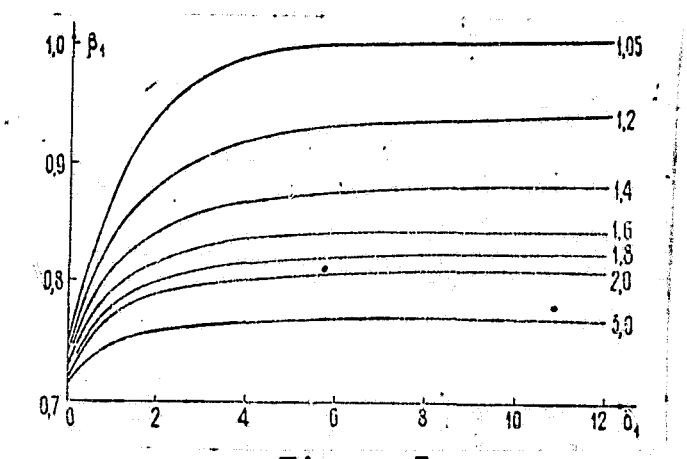

Figure 5.

It was found that the higher harmonics of the mean effective disk temperature are substantially weaker when compared with the corresponding harmonics of the effective temperature in the center of the disk. This means that the fluctuation of the mean disk radiotemperature can be adequately described by /1285 the first harmonic alone, and this is confirmed by the results of the measurements made of the integrated radiofrequency radiation from the moon on different wavelengths. That is

$$\overline{T}_e = \overline{T}_{e0} + \overline{T}_{e1}\cos(\Omega t - \overline{\xi}_1). \tag{21}$$

The magnitude $\bar{M}(\lambda) = \bar{T}_{e0}/\bar{T}_{e1}$, which, as will be seen from Eq. (20), has the form

$$\overline{M}(\lambda) = \frac{T_0(0)\,\beta_0}{T_1(0)\,\beta_1}\sqrt{1 + 2\delta_1 + 2\delta_1^2}. \tag{22}$$

can be used for purposes of comparison with the experiment.

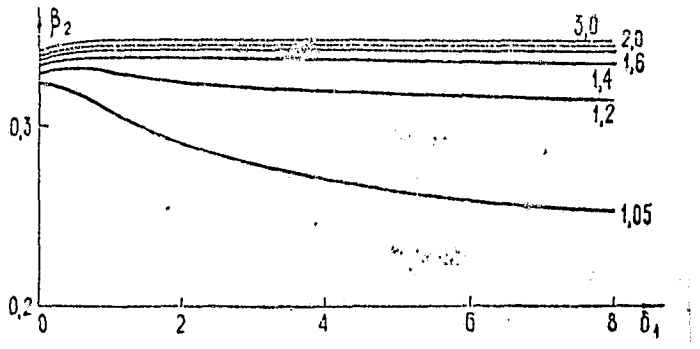

Figure 6.

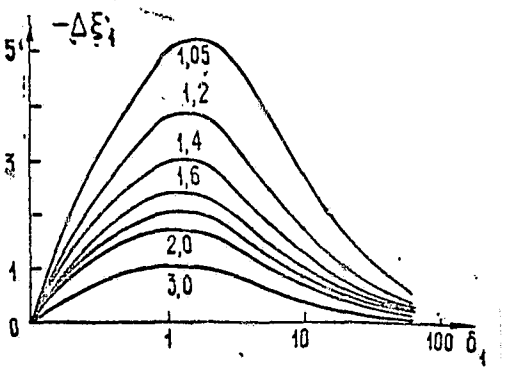

Figure 7.

2. The Spectrum of the Constant Component of the Integrated Radiofrequency Radiation from the Moon.

Precise measurements, made using the "artificial moon" method, detected an increase in the constant component of the integrated radiofrequency radiation on wavelength (see Figure 21) such that T_{e0} in Eq. (21) must be considered as a function of λ. As has already been pointed out in section II.2 of this survey, the increase in the constant component of the radiotemperature in the band of wavelengths from the infrared to $\lambda \simeq$ (2 to 3) cm, is the result of the weakness of the dependency of the thermal conductivity on the temperature.

The increase in the constant component in the wave band $\lambda > 3$ cm was explained by the presence of the heat flow from the moon's interior. Reference [32] includes the computation made for the constant component of the radio-

frequency radiation from the homogeneous surface layer of the moon when there is a flow of heat from the center. When references [33, 34] used the "artificial moon" method to measure radiotemperature the result was an estimate of heat flow density that proved to be close to the heat flow density for the earth. Further measurements showed that the temperature of radiofrequency radiation stopped increasing on wavelengths longer than 25 to 30 cm, apparently indicating a considerable compacting of the material at depths corresponding to the depth to which these waves penetrate.

Reference [29] contains the computation for the constant component of the integrated radiofrequency radiation from the moon when there is a heat flow from the center for a heterogeneous model of the structure in depth, and with the increase in the temperature in depth attributable to the temperature dependency of the thermal conductivity taken into consideration. The following dependence of $\overline{T}_e(\lambda)$ for $\lambda \gg hc'/kT$ was obtained for the two-layer model of the surface layer

$$T_e(\lambda) = [1 - R_\perp(\lambda)]\, A_0\, T_0(0) + [1 - R_\perp(\lambda)]\, qm\gamma_1 \times \qquad (23)$$
$$\times \sqrt{\frac{\tau}{\pi}\lambda}\,(A_1 - e^{-\gamma_1 d_2} A_2) + [1 - R_\perp(\lambda)]\, \Delta T_{\max} \frac{2\delta_1}{1+2\delta_1} B,$$

/1286

where

q is the density of the heat flow from the center;

$R_\perp(\lambda)$ is the power reflectance from the moon's surface [35];

d_2 is the thickness of the porous layer;

A_0, A_1, A_2, and B are coefficients that appear when averaging the moon's disk, and are complex functions of λ, d_2, and ϵ.

Figures 8 and 9 are included as examples of the dependence of the coefficients A_1 and A_2 on the wavelength, λ, for different values of d_2 and ϵ, and Figure 10 shows the theoretical curves constructed through Eq. (23).

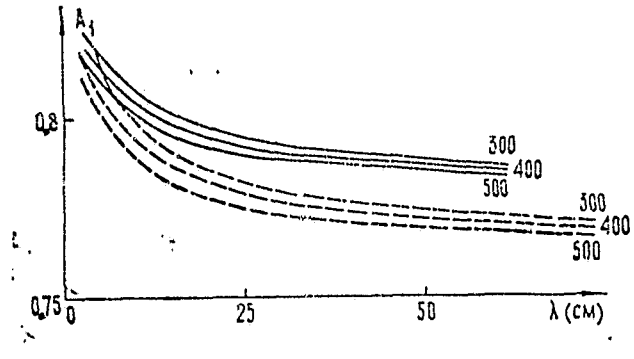

Figure 8. The coefficient A_1 in terms of λ when d_2 = 300, 400, and 500 cm; ε_1 = 2.25; ε_2 = 6 (the solid curves), and ε_2 = 7 (the dashed curves).

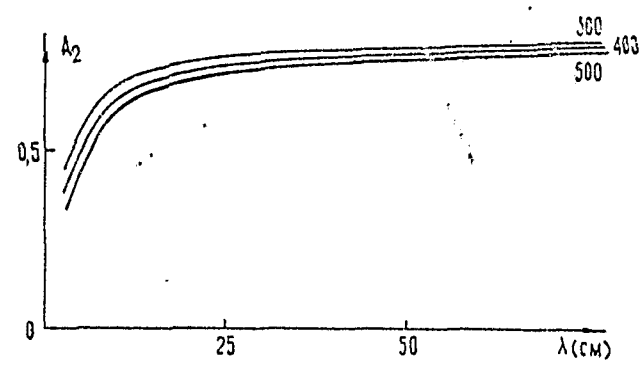

Figure 9. The coefficient A_2 in terms of λ when d_2 = 300, 400, and 500 cm; ε_1 = 2.25; ε_2 = 6.

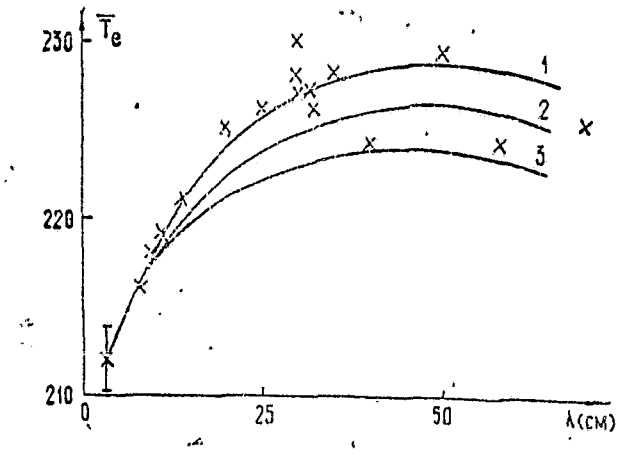

Figure 10. The effective temperature of the integrated radiofrequency radiation from the moon in terms of the wavelength for the following values of the parameters:

1. d_2 = 500 cm; $q = 0.65 \cdot 10^{-6}$ cal-cm^{-2}-sec^{-1};
2. d_2 = 400 cm; $q = 0.72 \cdot 10^{-6}$ cal-cm^{-2}-sec^{-1};
3. d_2 = 300 cm; $q = 0.8 \cdot 10^{-6}$ cal-cm^{-2}-sec^{-1}.

3. Radiofrequency Radiation From the Moon During Eclipse.

The theory behind radiofrequency radiation from the center of the lunar disk during eclipse is presented in references [18, 19]. Reference [19] contains precise and approximate expressions for the effective radiotemperature at the center of the disk in each of the four time intervals, t_k, listed in section II.2. The value of the relative maximum drop in the radiotemperature $\Delta T_e(t_3)/T_{em}$

which evidently occurs at the moment the umbral phase of the eclipse, t_3, occurs, is of interest for purposes of making a comparison with the experiment. According to [19], this magnitude equals

$$\frac{1}{M_e(\lambda)} = \frac{\Delta T_e(t_3)}{T_{em}} = -(1-R)\frac{4}{3\sqrt{\pi}}\frac{\varkappa a}{T_{em}}[\alpha_1(t_3-t_1)^{3/2}+(\alpha_2-\alpha_1)(t_3-t_2)^{3/2}] + \quad (24)$$

$$+(1-R)\frac{\varkappa^2 a^2}{2T_{em}}[\alpha_1(t_3-t_1)^2+(\alpha_2-\alpha_1)(t_3-t_2)^2] \quad \left(a=\sqrt{\frac{k}{\rho c}}\right).$$

/1287

What follows from Eq. (24) is that a change in the radiotemperature is determined by the magnitude of $\varkappa a = 2\pi b\sqrt{\varepsilon}/c\lambda\gamma$, and in the case of lunation depends on an analogous relationship between the electrical and thermal parameters of the material. Actually, as will be seen from Eq. (18), phase changes in the radiotemperature are proportional to the magnitude of $\gamma/\delta = 2\pi b\sqrt{\varepsilon}\sqrt{2\Omega}/c\gamma\lambda$. Thus, the inverse magnitude of the change in the radiotemperature, $M_e(\lambda)$, theoretically is almost a linear function of the wavelength, λ, and of the ratio of the thermal to the electrical parameters. The slope of the spectrum of $M_e(\lambda)$ is determined by the magnitude of γ/b. Figure 11 shows the theoretical $M_e(\lambda)$ curves computed through Eq. (24) for the 1963 eclipse with values for $\gamma/(b\sqrt{\varepsilon})$, equal to $7.3\cdot10^4$; $5.7\cdot10^1$ and $4.1\cdot10^4$.

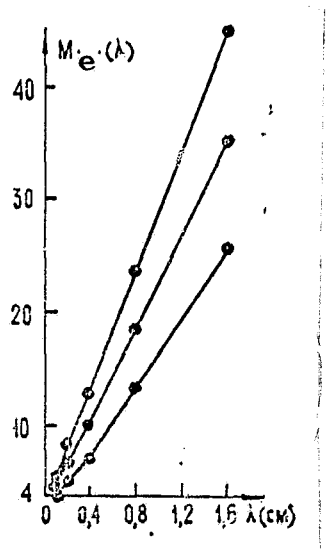

Figure 11.

It should be pointed out that the widths of the patterns of the antenna systems used in making the measurements were different, and therefore had different averaging effects. Reference [17] computed the integrated radiofrequency radiation from the moon and compared it with the radiofrequency radiation from the center of the disk during the 1963 eclipse in order to explain the applicability of the theory of radiation from the center of the lunar disk described above to a description of integrated radiation.

Figure 12 shows the relative changes that take place in the effective temperature at the center of the disk during eclipse at various wavelengths (the solid curves) and the corresponding changes in the mean effective disk temperature (the dashed curves). A comparison will show that the maximum relative drop in the temperature during eclipse, defined by the magnitude of γb, is practically the same in both cases. This means that

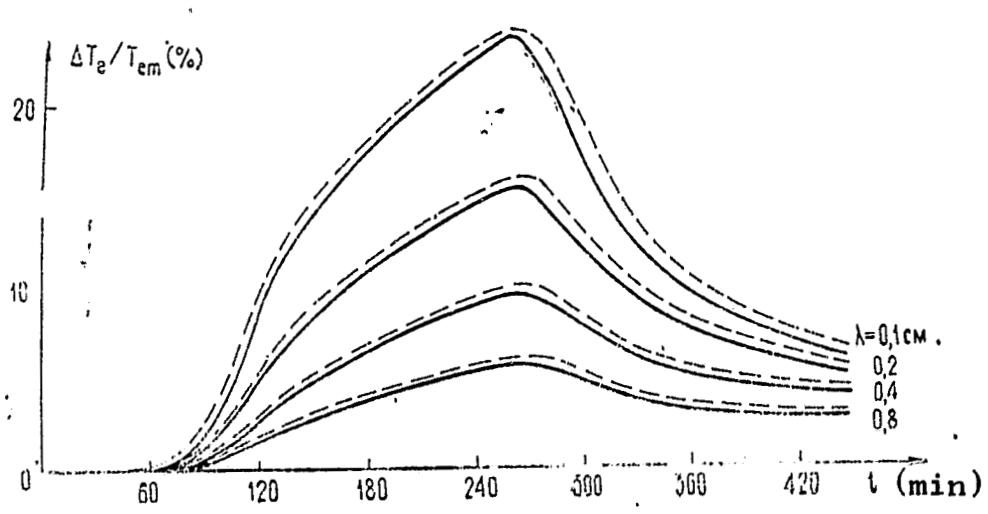

Figure 12.

in the case of eclipse the averaging effect of the antenna system pattern cannot /1288 be taken into consideration, and that the theory of radiofrequency radiation from an eclipsed moon developed in [19] for the center of the lunar disk can be used to define the magnitude of γb from experimental data.

IV. THE EMISSIVITY OF THE SURFACE OF THE MOON IN THE RADIOFREQUENCY REGION

1. Emissivity of a Smooth Surface

Emissivity of a flat body is understood to mean the ratio of the intensity of its emission in a particular direction to the maximum emission, assuming the emitting body is absolutely black. If the body is of a different form this definition yields the differential emissivity for a flat element of a surface, and the integrated emissivity for the body as a whole. In the case of smooth surfaces providing a mirror image, the differential emissivity is simply equal to $[1 - R(\varphi, \psi)]$, where $R(\varphi, \psi)$ is the Fresnel reflection coefficient for the specified direction of emission. Reference [36] assumed the surface of the moon to be smooth and obtained a mean spherical emissivity in terms of a constant component of integrated radiofrequency radiation

$$1 - \overline{R} = (1 - R_{\perp})\alpha, \tag{25}$$

where

$$R_{\perp} = \left(\frac{\sqrt{\varepsilon} - 1}{\sqrt{\varepsilon} + 1}\right)^2, \tag{26}$$

ε is the permittivity for the material;

α is a function of ε, and is given by the graph shown in Figure 13.

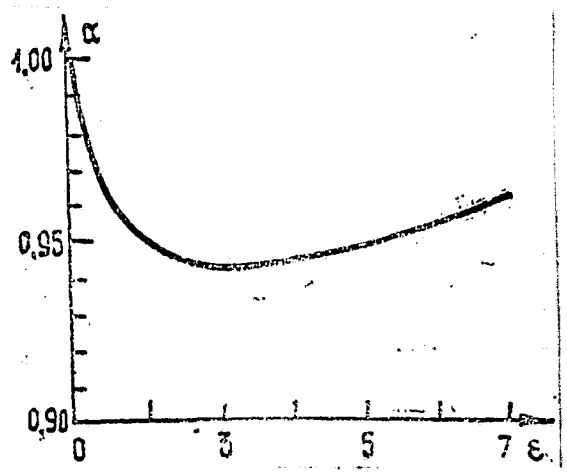

Figure 13.

In the general case the emissivity of the layer depends on the geometry of its surface (roughness) and on the change in the dielectric properties of the material in depth.

2. Emissivity of a Rough Surface

The real surface of any planet is uneven, so the following approximation is one in which consideration is given to the large-scale irregularities, the dimensions of which are significantly larger than the wavelength. The orientation of the individual small area has an arbitrary slope and can be characterized by the displacement of the normal to this small area from the smooth area in the middle of a surface. The introduction of these irregularities leads to the averaging of the emissivity for all values of the slopes of the small area within the limits of permissible angles of inclination [12, 37]:

$$\overline{1-R(\varphi,\psi)}=\int_{-\pi/2}^{+\pi/2}\int_{-\pi/2}^{+\pi/2}[1-R(\varphi+\Delta\varphi)(\psi+\Delta\psi)]\,W(\Delta\varphi,\Delta\psi)\,d(\Delta\varphi)\,d(\Delta\psi), \tag{27}$$

where

φ, ψ are coordinates defining the position of the small area on the rough surface;

$\Delta\varphi$, $\Delta\psi$ define the deflection of the normal to this small area from the normal to the smooth area in the middle of the surface;

$W(\Delta\varphi, \Delta\psi)$ is a function of the distribution of the angles of displacement from the normal.

References [37, 42] present the computations made on an electric computer of the Eq. (27) integral for the function $W(\Delta\varphi, \Delta\psi)$, with the shape of a Gaussian curve. The computations revealed that the contribution to emission from regions located near the edge of the disk increases with increase in the dispersion of the angles of inclination. There is very little dependence of emissivity on the degree of surface roughness in the central part of the disk.

The roughness of the surface must be taken into consideration when the reflection coefficient is established from radar measurements. As a matter of fact, radar methods make it possible to find the cross section of the backscattering for the moon, σ, which in the general case, can be described in the form

$$\sigma = gR_{\perp}\pi a^2. \tag{28}$$

Here

α is the radius of the moon,

$R_{\perp}$ is the power reflection coefficient in the case of normal incidence,

found through Eq. (26), and

g is a factor that takes the roughness of the surface into consideration.

Theoretically, the magnitude of g can be computed only for two limit cases; g = 1 when it is assumed that the moon's surface is smooth, and g = 8/3 when the condition is one with purely diffusion reflection. The reflection of radio waves from the moon's surface obviously is some intermediate case, so a whole series of assumptions usually enter into the estimate of the magnitude of g [104, 120]. At the same time, Eq. (28) makes it apparent that additional knowledge of the magnitude of g would make it possible to find the reflection coefficient for the moon's surface and from it to draw definite conclusions as to the nature of the moon's upper mantle.

Reference [38] contains an attempt to model backscattering for the moon in the optical band in order to explain the degree to which roughness effects the g factor. The backscattering of light from rough plates and spheres was investigated for this purpose. The roughness of the surface of the sphere was selected in such a way that its backscattering pattern in the optical band coincided with the analogous pattern for the moon at the selected wave in the radiofrequency band. Then the cross section of a rough and a smooth sphere was measured. The parameter g was taken as equal to unity for the smooth sphere. Consequently, $g = \sigma_r/\sigma_s$ for the rough sphere, and this magnitude was assumed equal to the analogous magnitude for the moon at the corresponding wave. The backscattering pattern for the sphere was defined in terms of the backscattering pattern for the plate made of the same material as the sphere. The roughness of the surfaces of both was made of the same materials. The results obtained for the moon were g = 1.6 when scattering was of waves in the centimeter band, and g = 1.06 when scattering was of decimeter waves.

3. Emissivity of the Surface Layer of the Moon Nonhomogeneous in Depth

Investigation of the natural radiofrequency radiation from the moon shows that the material of the upper mantle is nonhomogeneous in depth. The complex spectrum of the power reflection coefficient evidently should have a structure such as this. As a matter of fact, if the upper layer were less dense it would have a lower permittivity. Waves, the lengths of which are much shorter than the layer is thick, incident to the surface will be reflected from the

upper boundary of a medium with a vacuum. In the case of waves, the lengths of which are much longer than this layer is thick, it is just as if the layer is nonexistent, and these waves will be reflected from the lower, denser, layer. /1290 Accordingly, the reflection coefficient for a medium such as this will change in some interval of frequencies from the value of the reflection coefficient for the surface to its value for the sub-stratum.

As is known, the complex reflection coefficient for the surface with an arbitrary law for the change in parameters can be found through the Riccati equation [30]. Reference [35] resorted to an electronic computer solution of this equation to obtain the spectrum of the reflection coefficient for a layer, the density of which changes in depth in accordance with the exponential law

$$\rho(y) = \rho_2 - (\rho_2 - \rho_1)\exp(-y/y_0),$$

where

ρ_1 and ρ_2 are the density on the surface and in the depth, respectively. For all practical purposes the density reaches a maximum, $\rho = \rho_2$ at a depth of $y = 2.5y_0$. The following link between the thickness of a nonhomogeneous layer and the mean wavelength in the transition band was obtained

$$l = 2.5y_0 = \lambda_m/8.$$

Reference [39] includes spectra of the reflection coefficient for certain three-layer models of the moon's surface layer, found by numerical integration on an electronic computer. Taken into consideration during the computations was the frequency dependence of the permittivity [40] in accordance with Eqs. (32) and (33).

Figure 14 shows the spectrum of the reflection coefficient for a model of the surface layer, the qualitative change in the density of which in depth is shown by the graph in Figure 15. The computation was made using the following values for the parameters: $y_0 = 1.5$ cm; $\rho_1 = 0.7$ gram-cm^{-3}; $\rho_2 = 1$ gram-cm^{-3}; $\rho_3 = 2.5$ gram-cm^{-3}; $d_2 = 100$, 200, and 300 cm.

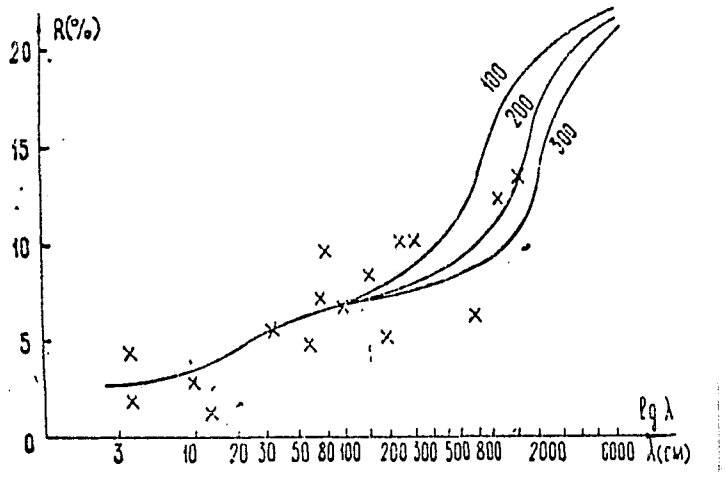

Figure 14. Spectrum of the reflection coefficient computed for a three-layer model of the surface layer of the moon.

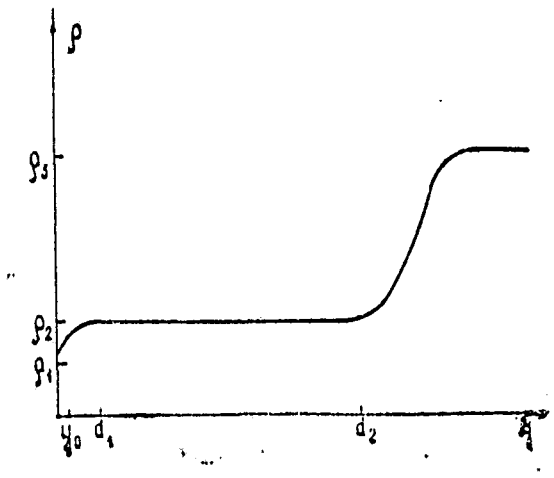

Figure 15. A model of the change in the density in depth in the surface layer of the moon.

4. Polarization of Radiofrequency Radiation from a Rough Surface

/1291

The magnitude of the coefficient of polarization of radiofrequency radiation from the moon in the most general case is equal to the ratio of the difference between effective temperatures, found for two mutually perpendicular orientations of the electrical vector for the antenna and averaged in terms of their patterns, to their sum [12]

$$p = \frac{\overline{T}^0_{e1} - \overline{T}^0_{e2}}{\overline{T}^0_{e1} + \overline{T}^0_{e2}}; \tag{29}$$

$$\overline{T}^0_e = \left\{ \int_{-\pi/2}^{+\pi/2} \int_{-\pi/2}^{+\pi/2} [\overline{R}_h(\varphi, \psi) - \overline{R}_v(\varphi, \psi)] \, [\sin^2(\gamma - \Delta) - \cos^2(\gamma - \Delta)] \, F(\varphi, \psi) T_e(\varphi, \psi, t) \right. \tag{30}$$

$$\left. \times \cos^2\psi \cos\varphi \, d\varphi \, d\psi \right\} \left\{ \int_{-\pi/2}^{+\pi/2} \int_{-\pi/2}^{+\pi/2} [\overline{R}_h(\varphi, \psi) + \overline{R}_v(\varphi, \psi)] F(\varphi, \psi) \cos^2\psi \cos\varphi \, d\varphi \, d\psi \right\}^{-1},$$

where

$\bar{R}_h(\varphi, \psi)$ and $\bar{R}_v(\varphi, \psi)$ are the mean statistical reflection coefficients for the vertical and horizontal polarizations, found through Eq. (27);

γ is the angle between the plane of the prime meridian and a projection on a map plane of the radius vector directed from the center of the moon to a point with coordinates φ, ψ;

Δ is the angle between the plane of the electrical vector for the antenna and the plane of the prime meridian;

$T_e(\varphi, \psi, t)$ is the effective temperature of the section under consideration for the case of an absolutely black moon;

$F(\varphi, \psi)$ is the receiving antenna pattern.

As will be seen from Eq. (30), there are three magnitudes that define the coefficient of polarization; temperature distribution $T_e(\varphi, \psi, t)$, pattern $F(\varphi, \psi)$, and emissivity $\overline{1 - R(\varphi, \psi)}$.

Reference [12] estimates the coefficient of polarization for the radiation from the moon in the case when the surface of the moon is smooth, the antenna pattern is wide as compared with the angular dimensions of the disk of the planet ($F(\varphi, \psi)$ = constant), and $T_e(\varphi, \psi, t)$ is the sum of the constant component and the first harmonic of the radiotemperature. It is shown that the degree of polarization of the integrated radiofrequency radiation from the moon is determined solely by the deviation of the distribution of temperature over the disk from the central, symmetrical distribution, and in particular, by the degree of the drop in the temperature toward the lunar pole.

Reference [41] is devoted to the question of the polarization of the integrated radiation from the moon, and assumes that the moon's surface has large-scale unevennesses. The computations made showed that the magnitude of the coefficient of polarization depends on the phase of the moon, reaching a maximum near quadrature. The variable component of the polarization decreases with increase in the wavelength, and vanishes, for all practical purposes, when λ = 3.2 cm.

References [43-48] review the question of averaging the effect of the antenna pattern when measuring polarization. Reference [46] assumed that the pattern is a body of revolution, the cross section of which has the shape of a Gaussian curve. Figure 16 shows the change in the coefficient of polarization along the radius of the disk of the moon for various values of pattern width θ at the half power level. It was assumed that the surface of the moon was ideally smooth. As will be seen, the coefficient of polarization has practically no dependence on the pattern width in the central region of the disk bounded by a circle with radius $0.6R_m$. Figure 17 shows the results of the computation for p when ϵ = 1.5 and 3, for different values for the dispersion σ. The /1292

coefficient of polarization has practically no dependence on the magnitude of σ for $r/R_m < 0.6$. The effect of roughness appears only near the limb of the moon.

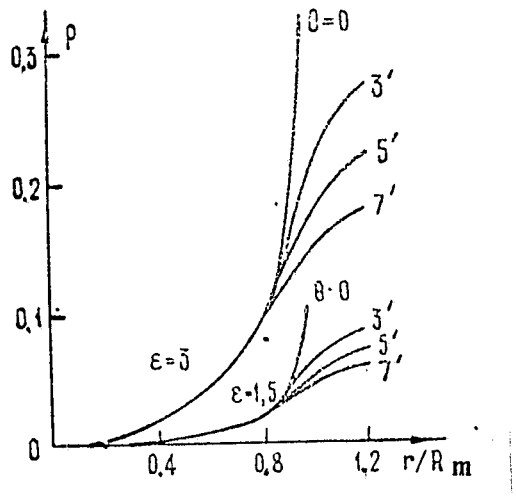

Figure 16. Change in the coefficient of polarization along the radius of the disk of the moon when θ = 0, 3', 5', and 7' and ϵ = 3, 1.5.

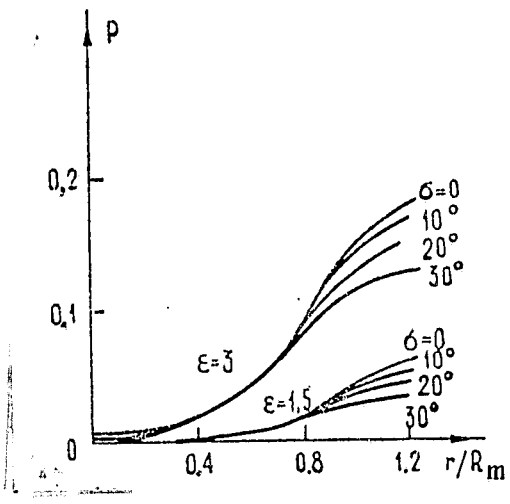

Figure 17. Change in the coefficient of polarization along the radius of the disk of the moon when θ = 7', σ = 0, 10, 20, 30° and ϵ = 3, 1.5.

References [43-45, 47] contain the polarized characteristics of the radio-frequency radiation from the moon as received by an antenna with a beavertail pattern. The case of roughness with uniform distribution of the angles of inclination within definite limits without consideration for shading, something that is a very rough approximation, has been considered [43-45]. Reference [47] took up shading, and assumed that the statistics on angles of inclination for unevennesses are subordinate to a normal law. The computations showed that during passage of the pattern for the central part of the lunar disk what is observed is vertical polarization, but that the coefficient of polarization does not depend on σ and θ to any great extent. Polarization is horizontal near the limb of the moon, and here the coefficient of polarization has a significant dependence on the width of the pattern in a narrow section and on the dispersion of the angles of inclination for the unevennesses.

References [45-48] contain analyses of the polarized characteristics of radiofrequency radiation from the moon with account being taken of the averaging

effect of the multilobed pattern that can be formed by using a two-element radio interferometer. It is shown that the measurement of the coefficient of polarization by the interferometer is desirable to make when n = 1.5 (n is the number of lobes that can be fitted to the disk of the moon), where the effect of ε and σ is the most marked.

Thus, the computations made show that the measurement of the coefficient of polarization in the central region ($r/R_m < 0.6$) makes it possible to find the permittivity of the surface layer of the moon. The effect of roughness shows up only near the limb of the moon, so it is possible, after first finding ε, to estimate the degree of roughness of the lunar surface from the value of the coefficient of polarization near the limb.

V. RESULTS OF MEASUREMENTS OF NATURAL RADIATION FROM THE MOON

1. Results of Infrared Measurements

Pettit and Nicolson [1] made the earliest measurements of the natural radiation from the moon in the infrared band, and these were extremely significant in investigating this radiation. They obtained the temperature of the sub- /1293
solar point, the midnight temperature, the distribution of the intensity of disk radiation during full moon, and change in temperature of small areas near the center of the disk and near the limb during eclipse.

The improvement made in the sensitivity of receivers in the infrared band has made it possible to conduct a series of observations with high resolution. Figure 18 shows the results of measurements made of temperature on the surface of a small area on the lunar equator during lunation [49]. Sinton, et al., used a narrow-band filter on λ = 8.8 microns, in making the daytime temperature measurements (see [49], for example). Maps of isotherms of the illuminated surface were obtained for nine phase angles with a resolution of 25 seconds of arc (1 second of arc is of the order of 1/1800 of the lunar diameter). Saari and Shorthill [49] also measured the daytime temperature with a high resolution of 1 second of arc. The measurements were made in the long wave interval λ = (10 to 12) microns for 23 values of phase angles.

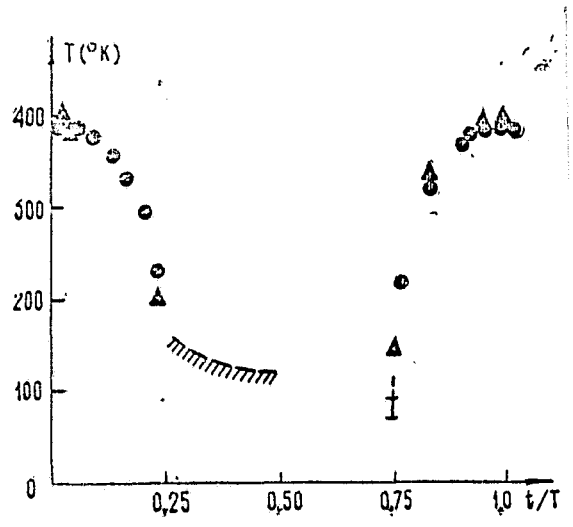

Figure 18. Change in the surface temperature in the center of the lunar disk from experimental data:
▲▲▲ - Sinton, et al. [49];
●●● - Saari and Shorthill [49];
III - Low [51].

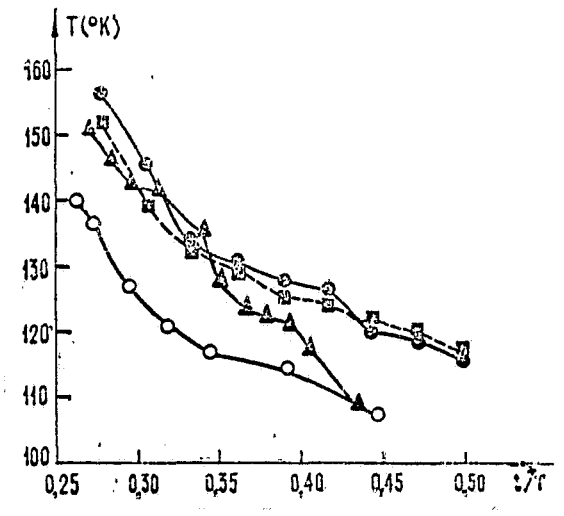

Figure 19. Change in the surface temperature at the center of the disk during the lunar night from experimental data:
●●●, ■■■ - Surveyor V [49];
▲▲▲ - Shorthill and Saari [49];
ooo - Murray and Wildey [50].

The temperature of the lunar surface after the sun has set has not been as well studied because these measurements require more sensitive instruments. The hatched region in Figure 18 is shown in more detail in Figure 19. The measurements made by Murray and Wildey [50] were in the λ = (8 to 13) microns interval of wavelengths, with resolution 26 seconds of arc. Extrapolation of these results to $t/T = 0.5$ provides an estimate for the midnight temperature of the surface of the moon $T_n \sim 104°$. The data obtained by Surveyor V [49] are considered to be the absolute upper limit of the night temperature. However, [130] points out that a more detailed analysis of these results, taking into consideration all the errors that possibly could have been made in the measurements, makes it possible to eliminate the disparity between the Surveyor V data and the results obtained from ground measurements. Low [51] made some measurement just before sunrise on λ = 17.5 microns. It turned out that the mean temperature of the surface was 90°, although there is a region where the temperature is below 70°.

Interesting results were obtained from the measurements made of the cooling of the lunar surface during the eclipse of 19 September 1964. Measurements were made by two groups; Saari and Shorthill [52], and Ingrao, Young, and Linsky [26]. Figure 20 shows the results obtained by the second group. The dark circles describe the cooling of the regions 30 seconds of arc to the east and west of the crater Tycho, and the light circles describe the cooling of the region inside the crater Tycho. As will be seen from Figure 20, the interior of the crater cools more slowly during lunar eclipse than do the surrounding areas. Craters such as these appeared quite brightly in the infrared photography of lunar eclipses, and so are called "hot spots" in the literature. To date, 330 similar bright regions have been detected. They have been classified in order to establish a link with the visual anomalies of the relief. The results of this classification have shown that some 90% of all "hot spots" are linked with craters, which appear lighter even during full moon. Some 10% of the spots have no connection with any anomalies of the relief. /1294

The literature discusses the following possible explanations for the phenomenon observed.

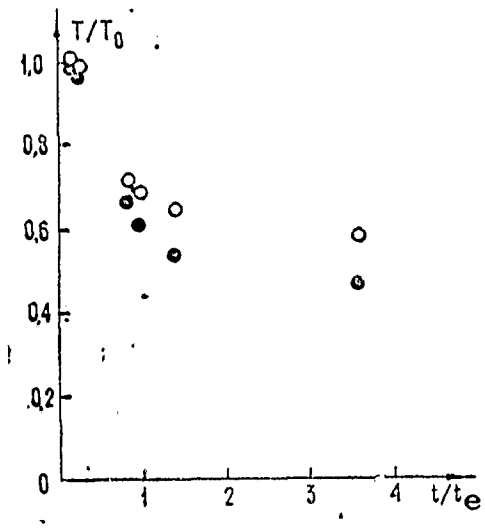

Figure 20. Change in temperature of the surface during the eclipse of 19 December 1964, from experimental data:

ooo - the crater Tycho;
●●● - region around the crater Tycho.

1. Different emissivity for individual small areas on the surface of the moon [53]. However, as estimates have shown, the emissivity of small areas should differ by a factor of two in order to provide the necessary difference in temperatures of tens of degrees.

2. Difference in transparency of the material of small areas in the infrared band [54]. But the obvious objection here is the same as that advanced in connection with the preceding hypothesis; too great a difference is needed in the transparency of the individual small areas.

3. The existence of internal heat sources. The objection to this hypothesis is that anomalous regions often do not appear to be any warmer during the lunar day.

4. Scattering on the rough surface. A surface covered with roughnesses of the order of several centimeters will appear to be warmer than a flat surface made up of the same rocks [23, 55].

5. The upswelling of denser material [53]. This structure should produce warm anomalies and seems to be the more probable. But computations have shown [21] that the temperature of the "hot spots" should be substantially higher than that observed in the case of purely rocky surfaces.

2. A Method for Making Precise Measurements of Radiofrequency Radiation from the Moon (the "Artificial Moon" Method). /1295

The effective temperature of the radiofrequency radiation from the moon, $\bar{T}_e$, is proportional to signal strength at the antenna output, measured by radiometers. The proportionality factor is determined by the antenna parameters (directivity, losses in the antenna plumbing, pattern). Difficulty in establishing these parameters results in significant errors in the measurements. The accuracy of finding $\bar{T}_e$ by these direct methods usually is not more than 10 to 20%, so the use of radio data to establish the physical parameters of the surface layer of the moon is severely limited.

Most of the experimental results on natural radiofrequency radiation from the moon, and included in what follows, were obtained by the precise "artificial moon" method [57]. This method is based on comparing the radiofrequency radiation from the moon with known radiofrequency radiation from an absolutely black disk placed in the Fraunhofer zone of the antenna (distance from the telescope $R \geq D^2/\lambda$, where D is the diameter of the mirror, λ is the wavelength) at a sufficiently large angle of elevation, h_d, to the sky background. The signal strength at the disk is proportional to the known magnitude

$$T_d \int_{\Omega_d} F d\Omega,$$

where

T_d is the temperature of the disk, equal to the ambient temperature;

F is the antenna pattern;

Ω_d is the angular size of the disk, as seen from the aperture of the antennas.

The entire system can be calibrated quite easily by using this magnitude. There is no need to measure the antenna output power, and only accurately known antenna parameters are used.

It was found that the most significant error in the method is associated with the effect created by radiofrequency radiation from the earth, and by nonuniform radiation from the sky. These diffract at the disk and enter the radio telescope, increasing the standard signal to an indeterminate magnitude. Reference [57] has shown that the use of two additional screens, a black disk,

and a hole in a black face (the diameter of the hole exactly equal to the diameter of the disk), eliminates the diffraction error. Use of a second standard helped find the conditions for installing the disk such that the effect of the earth's radiofrequency radiation could be reduced to the absolute minimum.

References [58, 59] made the computation for the correction factors for diffraction at the disk attributable to radiation from the earth and from the background. All of this resulted in later use of just the standard disk to measure radiofrequency radiation from the moon. The "artificial moon" method has made it possible to find the temperature of the integrated radiofrequency radiation from the moon with an accuracy of within 2 to 3% over a broad band of wavelengths.

3. Experimental Data on Radiofrequency Radiation from the Moon During Lunation and During Eclipse

There is, today, much experimental material on the natural radiofrequency radiation from the moon during lunation in a broad band of wavelengths between 0.7 mm and 150 cm. The results of these measurements are listed in Table 1.

As will be seen from Eq. (21), it is desirable to characterize the natural radiofrequency radiation from the moon by the spectra of three magnitudes: the constant component; the amplitude of the first harmonic; and the radiotemperature phase lag in terms of the optical phase. The spectrum of the constant component of the integrated radiofrequency radiation is obtained in the main by the method of precise measurements, using the "artificial moon" [32, 57, 60 - 62, 64 - 71, 75 - 80, 82 - 86], as shown in Figure 21. The spectrum of the amplitude of the first harmonic, characterized by the relationship $\bar{M}(\lambda) = \bar{T}_{e0}(\lambda)/\bar{T}_{e1}(\lambda)$, is shown in Figure 22 [2, 57, 60 - 92], from which it will be seen that at wavelengths longer than 15 to 20 centimeters the variation in radiation intensity practically disappears. Figure 23 shows the spectrum of the first harmonic phase lage $\bar{\xi}_1(\lambda)$ [2, 57, 60 - 92]. /1297

TABLE 1.

Measurement No.	λ (cm)	T_{e0} (°K)	T_{e1} (°K)	ξ_1 (degrees)	Measurement error (± %)	Half-width of the pattern	Authors
1	2	3	4	5	6	7	8
1	0,087	191	140	5	15	11	Fedoseyev et al. [131]
2	0,108	199	117	15	12	13,5	" [131]
3	0,126	179	119,5	5	12	8	" [131]
4	0,13	219	120	16	15	10	Fedoseyev [85]
5	0,145	180	110	2	15	18,5	Kukin, Fedoseyev [131]
6	0,18	240	115	14	20	6	Naumob [84]
7	0,225	201	80	18	10	10	Kislyakov, Naumov (in print)
8	0,40	230	73	24	10	25	Kislyakov [79]
9	0,40	228	85	27	15	1,6	Kislyakov, Solomonovich [91]
10	0,40	204	56	23	4	36	Kislyakov, Plechkov [132]
11	0,8	197	32	40	10	18	Solomonovich [76]
12	0,8	211	40	30	15	2	Solomonovich, Losovskiy [89]
13	0,86	180	35	35	15	12	Gibson [94]
14	1,25	215	36	45	10	45	Piddington, Minnet [72]
15	1,25	222	40	64	5	40	Plechkov [100]
16	1,45	215	36	37	5	40	" [100]
17	1,63	208	37	30	3	44	Kamenskaya et al. [99]
18	1,63	207	32	10	3	44	Dmitrenko et al [66]
19	1,8	202	24	30	5	63	Plechkov [100]
20	2,0	206	19	56	5	60	" [100]
21	2,0	190	20	40	7,5	4	Solomonovich, Koshchenko [88]
22	2,5	210	15,5	42	5	72	Plechkov [100]
23	3,15	195	12	44	15	9	Mayer et al. [93]
24	3.2	223	17	45	15	6	Koshchenko et al. [87]
25	3,2	245	16	41	15	40	Strezhneva, Troitskiy [80]
26	3,2	210	13,5	55	2,5	72	Krotikov et al. [57]
27	3,2	213	14	26	2	87	Bondar' et al. [60]
28	3,2	216	16	15	3	40	" [60]
29	7,93	216	7	45	3,5	73	Alekseyev et al. [69]
30	9,4	220	5,5		5	140	Medd, Broten [81]
31	9,6	218	7	40	2,5	100	Krotikov [62]
32	11	214			12	17	Messger, Strassl [56]
33	11	219	6	55	3	110	Alekseyev et al [69]
34	14,2	221	—	—	2,5	140	" " [63]
35	20,8	225	—	—	2,5	200	" " [69]
36	20,8	205	5	36			Waak [133]
37	21	217	5,3	48	2	36	" [133]
38	21	250	5		15	35	Messger, Strassl [56]
39	23	254	6,5		15	38	Castelli et al. [97]
40	25	226	—	—	3	180	Alekseyev et al. [71]
41	30,2	227	—	—	3,5	210	" " [71]
42	32,3	233	—	—	2,5	180	Razin, Fedorov [86]
43	35	236	—	—	4	186	Krotikov et al [61]
44	36	237	—	—	3	190	" " [64]
45	40	224	—	—	5	40	" " [64]
46	50	229	—	—	3	280	" [65]
47	58	224	—	—	—	—	Troitskiy et al. [83]
48	70,16	225	—	—	3,5	90	Krotikov et al [68]
49	168	233			4	13,6·4°	Baldwin [134]

Commas represent decimal points.

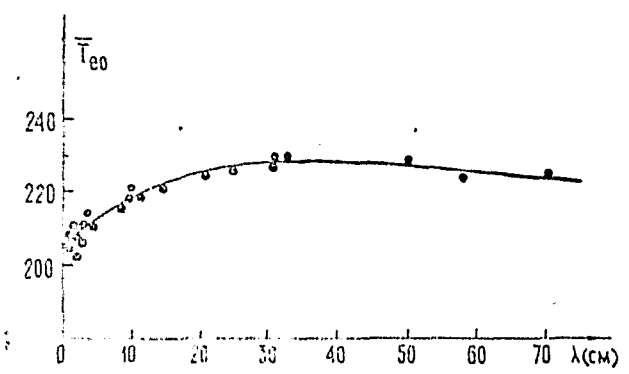

Figure 21. Experimental spectrum of the constant component of the integrated radio-frequency radiation.

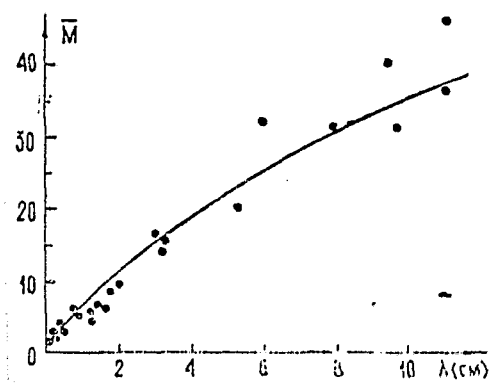

Figure 22. Experimental spectrum $\bar{M} = \bar{T}_{e0}(\lambda)/\bar{T}_{e1}(\lambda)$.

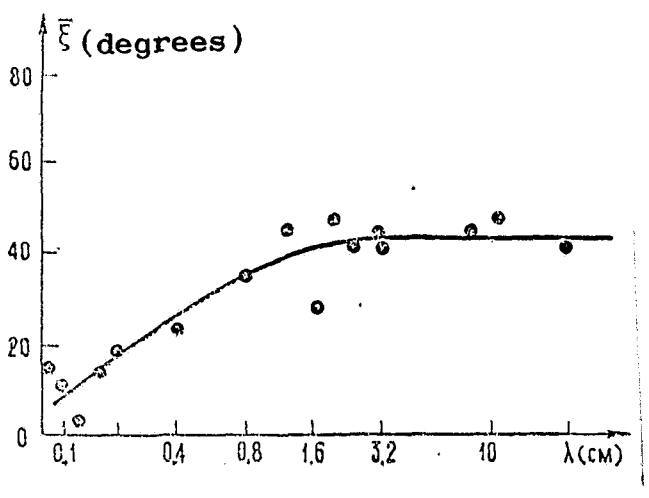

Figure 23. Experimental spectrum of first harmonic phase lag.

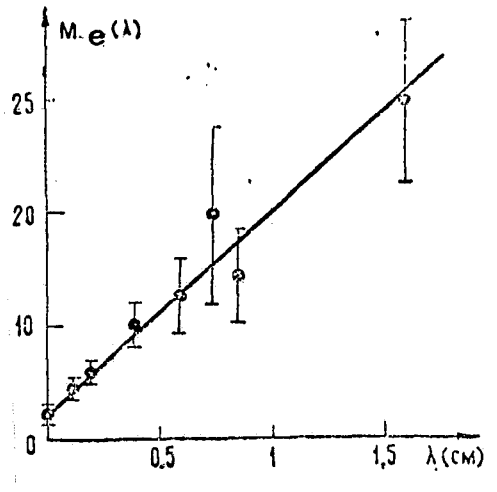

Figure 24. Experimental spectrum $\bar{M}_e = \bar{T}_{em}/\Delta\bar{T}_e$.

Important information on the properties of the material of the upper mantle is contained in the data on change in radiation intensity during lunar eclipses [1, 13 - 20, 95 - 100]. These data are shown in Figure 24, where th magnitude of $\bar{M}_e = \bar{T}_{em}/\Delta\bar{T}_e$, equal to the inverse magnitude of the maximum relative decrease in intensity characteristic of the end of the dark phase of the eclipse for the center of the disk of the moon, is plotted along the y axis. As will be seen from this figure, there is practically no change in intensity during eclipse at wavelengths longer than 1.5 centimeters.

VI. RESULTS OF THE MEASUREMENT OF THE SPECTRUM OF THE REFLECTION COEFFICIENT

The spectrum of the reflection coefficient is quite a significant characteristic of the surface layer of the moon. Values for the reflection coefficient over a broad band of wavelengths have been obtained by radio astronomy methods, as well as by radar methods. There are several radio astronomy methods that can be used to find the reflection coefficient, including, for example, methods involving the constant component of the radiotemperature [36], the polarization of natural radiation [102, 43-48], and the distribution of the brightness temperature over the disk [37, 89, 101]. However, radar measurements, made over a broader band of wavelengths, make the principal contribution to the results obtained in investigating the spectrum of the reflection coefficient [103-109]. /1298

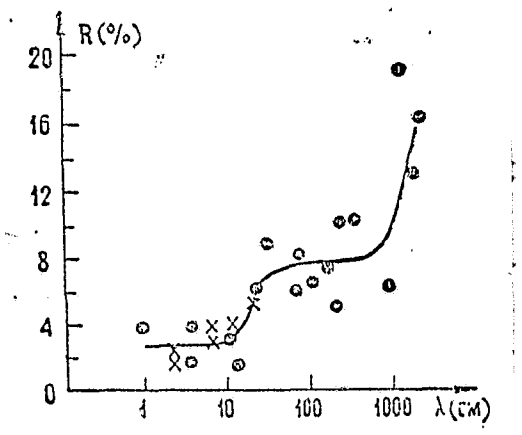

Figure 25. Experimental spectrum of the reflection coefficient.

The circles in Figure 25 are the values of the local reflection coefficient, reduced to the corresponding g values indicated in section IV.1 of this survey. The xs in the figure are plots of data obtained from measurements made of the polarization of the radiofrequency radiation.

VII. LABORATORY INVESTIGATIONS OF TERRESTRIAL ROCKS

The natural assumption of identity of rocks comprising the upper mantles of the moon and of the earth led to numerous laboratory investigations of terrestrial rocks. Such characteristics as lightness, color, albedo, scattering indicatrices, backscattering curves, polarization of reflected light, and behavior of reflectivity over the spectrum were compared in the optical band of wavelengths. Barabashev and Chekirda [110] obtained a mass of experimental material that led them to conclude that the lunar surface apparently was covered by tufa-like rocks badly fragmented into grains 3 to 10 millimeters in size. Reference [111] contains the results of albedo measurements and backscattering curves for 200 different surfaces; rocks, metals, natural surfaces, such as grass, lichen, moss, and artificial surfaces, such as wire wound on a flat surface, and the like. Comparisons made with lunar backscattering curves led the authors to conclude that the lunar surface is covered with rock dust, the grain sizes of which are between 10 and 15 microns, and which forms a complex porous structure under lunar vacuum conditions. Hapke [112] explains the narrower albedo of lunar rocks as compared with terrestrial rocks by bombardment by fast particles. Lyot [113], and later on Dollfus [114], made careful measurements of the polarization of the light reflected by the moon, and by various terrestrial rocks, and the results led them to conclude that the surface of the moon probably was covered by a thin layer of volcanic dust, or ash.

However, all of the optical comparison methods listed in the foregoing can only provide information on the thin surface layer, the properties of which can differ from the properties of the deeper layers. Moreover, these methods do not allow a determination to be made of the chemical nature of the material. As a matter of fact, characteristics such as scattering and polarization of light during reflection depend on the geometry of the surface, on the nature of the roughness, rather than primarily on the composition of the surface. For example, reference [111] cites the fact that backscattering curves for lichen, the surface of which has a porous structure, are much like the lunar curves. It is obvious that the only way to establish from the earth the chemical composition of the material forming the upper mantle of the moon is /1299 to compare the electrical characteristics of the lunar surface with the corresponding characteristics of terrestrial rocks. The method that evaluates the

chemical material of the moon from radio astronomy data is based on the assumption that the solid material of the moon is composed of silicate rocks, as is the case on earth.

Measurements made of the tangent of the angle of loss, tan Δ, and of the permittivity ϵ, for different rocks have shown that these magnitudes are very much dependent on the chemical compositions, and therefore can serve to establish that composition. However, we also know that the parameters tan Δ and ϵ depend on the density of the rock, as well as on the chemical composition. In this connection, [16] has pointed out that in order to make any comparison it is necessary to use certain functions of tan Δ and ϵ that will not depend on the density of the material, that is, functions that will be invariants of the density. Theoretical, as well as wide-ranging experimental investigations of volcanic rocks [115] have shown with sufficient accuracy that the magnitudes tan $\Delta/\rho = b$ and

$$(\sqrt{\varepsilon} - 1)/\rho = a \tag{31}$$

do not depend on the density, ρ, over a broad range of change in density. The measurements detected quite a clear-cut dependence of $b = \tan \Delta/\rho$ on the amount of SiO_2 in the rock.

The relationship obtained served for estimating the SiO_2 content in the lunar material, with the results found to be 55 to 65% by weight [115-118]. Special experimental investigations of rocks, carried out in the band between 30 and 500 megahertz [40], revealed that the magnitudes of b and a can be established primarily by the chemical composition of the rocks, and in part, by the type of crystalline structure; in other words, by the history of the formation of the rocks (intrusive, effusive). It was found that the magnitude of b changes by a factor of more than 20 rocks from acid to basic, and that the magnitude of a changes by a factor of 2.5, from 0.45 for acid to 1.1 for ultra-basic rocks. The magnitude of b has practically no dependence on the frequency in the centimeter and decimeter bands, yet a exhibits a marked frequency dependence. The following empirical formula can be used for the frequency dependency, averaged for all rocks

$$a(\lambda) = a_0 + \xi \lg \lambda/\lambda_0. \tag{32}$$

The mean value for all rocks is $a_0 = 0.5$, as has been shown by measurements made of various terrestrial rocks at a wavelength of $\lambda_0 = 3$ centimeters. Eq. (31) [sic] will therefore be in the form

$$a(\lambda) = 0.5 + 0.045 \lg \lambda/3. \qquad (33)$$

Analysis of the values for b and a obtained in [40] revealed that on the average, the dependence on the concentration of the particular oxide in the rock established for them will hold. The most desirable way to depict this dependency is in a form similar to the Harker variation diagram [118]. The magnitude of a, or of b, for some particular rock is plotted on the X axis, and the values of oxides contained in the rock are plotted on the Y axis. The result is the diagram for certain intrusive rocks shown in Figure 26 [119]. Data on the chemical composition of the rock used to contruct the diagram were taken primarily from typical analyses for the type of rock under consideration and contained in the literature on the subject.

The presence of a behavorial association between the b and a parameters and the chemical composition is the result of the fact that the variation in the composition of the rocks is not an arbitrary one. There is no such thing as silicate rocks with an arbitrary content of various oxides. A reduction in the SiO_2 content in the transition from one rock to another, for example, will on the average, result in definite changes taking place in the content of one, /1300 or of several of the other oxides. What this means in fact, for example, is that the percentage content of SiO_2 in a rock will, on the average, determine the content of the rest of the oxides, and accordingly, the type of rock.

Measurements of permittivity and tangent of the angle of loss for a number of rocks were recently using frequencies of 35 and 450 gigahertz [128]. The data obtained are in good concordance with the above-mentioned assumption concerning the dependence of electrical properties on the chemical composition of the substance and the frequency.

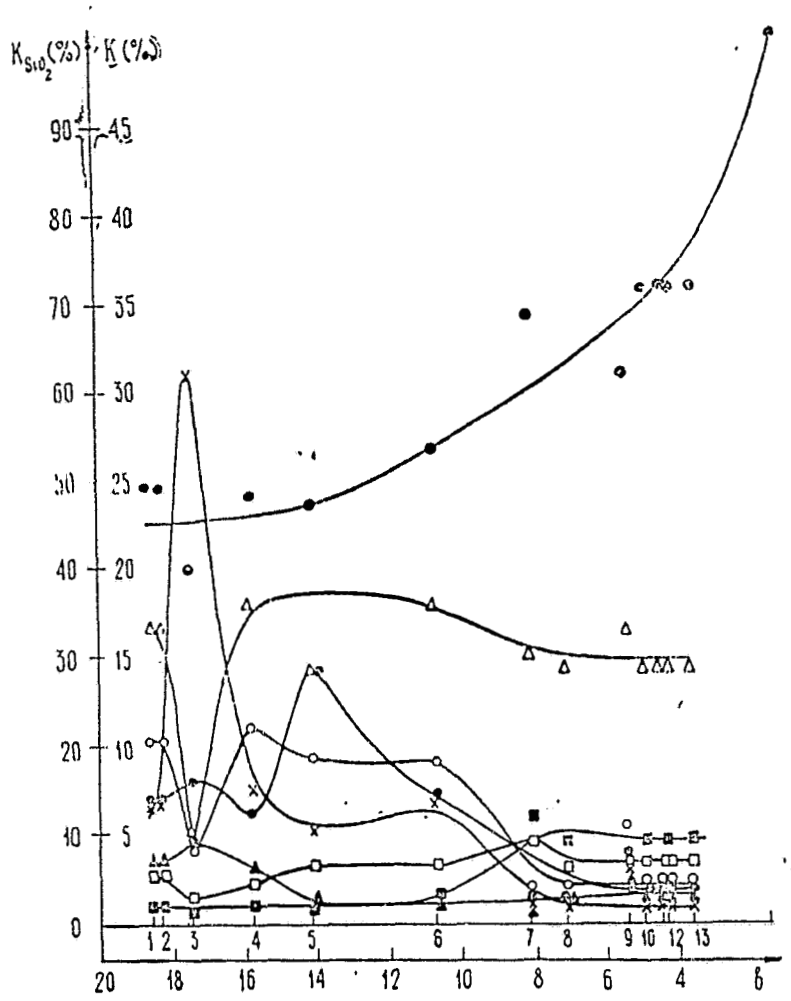

Figure 26. Variation diagram of losses for volcanic intrusive rocks:

1- gabbro-diabase No. 1; 2- gabbro-diabase No. 2;
3- peridotite; 4- gabbro No. 1;
5- gabbro-diabase No. 3; 6- gabbro No. 2;
7- granite-haplite; 8- granite No. 1;
9- quartz diorite; 10- granite No. 2;
11- granite No. 3; 12- granite, medium-sized;
13- granite No. 4.

The dependence of the specific tangent of the angle of loss on the percentage content in the rock: ●●● - SiO_2; ΔΔΔ - Al_2O_3, etc.

VIII. INTERPRETATION OF THE DATA ON NATURAL AND REFLECTED RADIATION, AND ON THE STRUCTURE AND PROPERTIES OF THE UPPER MANTLE OF THE MOON

/1301

Let us now consider, briefly, methods for use in interpreting experimental data on natural radiation and reflection of radio waves in order to obtain information on the properties and the structure of the material of which the upper mantle of the moon is made. But we will not go into detail on how the computations in the various papers were made, but will, instead, limit ourselves to a description of the physical aspects involved in the analysis.

The set of equations (1) to (3), (14), and (15) fully establish the natural radiation from the moon. Therefore, it is possible (at least in principle) to establish all the parameters of the material included in the equation from the various characteristics of the radiation. To this end, it is customary to seek a solution for a family of values for the parameters which then can be established by comparing the computation with an experiment. This is possible, as a practical matter, when the solution depends on just one parameter. We, however, have some ten unknowns (k, c, ρ, ε, d, q, etc.), the majority of which are functions of the depth in the general case, and sometimes even are functions of the temperature. The method used for the analysis therefore should be one that will select the characteristics of the radiation that can be established by one parameter, for the most part. The other parameters should have no effect, or so weak an effect that it can be ignored in the first approximation.

As soon as this selection, based on theoretical analysis, has been made the particular parameter for the observed phenomenon is eatablished; that is, the corresponding special model is constructed to explain the characteristic of the radiation, or the group of characteristics. The selection of special models that explain all of the available experimental material results in the creation of the general model best satisfying all of the data. This has been precisely the approach used to study the moon. Let us, at this point, consider the concrete results of the interpretation.

1. Quasi-Homogeneity of the Properties of the Material in Depth

The possibility of finding sharp inhomogeneities in the surface layer in depth is associated with the variable thermal regime, and with the fact that

the data from measurements of intensity at different wavelengths correspond to the measurement of temperature at different depths. The layer is sounded, so to speak, in depth when the wavelength of the received radiation is lengthened. Any sharp changes in the properties of the upper mantle with depth will result in a change in the temperature distribution and therefore can be detected in the spectrum of the radiofrequency radiation. Because substantial temperature gradients are present in the upper layer with thickness 3 to 4 t_T, the result of the solar flux, study of this layer is easiest. (The spectra of the amplitude of the first harmonic and of the phase lag, for example, are informative only of a layer of an order of thickness of a few tens of centimeters). But, as we shall see in what follows, because of the considerable flow of heat from the interior of the moon, and because of the low thermal conductivity of the material of the upper layer, investigation of the surface layer to considerable depths is possible.

Analysis of the spectrum of the amplitude of the first harmonic of the radiotemperature (Figure 22) has revealed that it well satisfies homogeneous models of the surface layer, and does not in any way correlate to sharply inhomogeneous models, assuming the existence of a dust layer a few millimeters thick covering dense rocks [16]. The spectrum of the first harmonic phase lag, $\xi_1(\lambda)$ (Figure 23), also is indicative of the approximately homogeneous distribution of thermal properties of the material in depth. /1302 The maximum phase lag is 45° when λ is lengthened. This is precisely the magnitude obtained in the theory of homogeneous models [12]. Any significant increase in the inhomogeneity, particularly in that of the dust layer, will result in a marked increase in the maximum delay [72]. Thus, the quasi-homogeneous model of the very topmost layer is in quite good concordance with the spectrum of natural radiation.

2. The Thermal Parameter γ

As we pointed out in section II.1, of this survey, a homogeneous model in which the properties did not depend on temperature, and in which they did not change with depth, was used to compute the thermal regime for the surface in the first approximation. Considered in the second approximation was a homogeneous model with thermal conductivity and specific heat dependent on temperature.

Today, as a result of measurements made, we know quite accurately that the midnight temperature of the surface is $T_m = 100°K$, that the noon temperature is $T_n = 395°K$, that the ratio of the constant component to the amplitude of the first harmonic of the integrated radiation is $T_0/T_1 = 1.3$ when $\lambda = 0$, that is, in the infrared band (see Figure 22), and that the relative drop in the temperature during eclipse (in the same band) is $\Delta T_e/T_{em} = 0.52$ (see Figure 24). Comparison of these magnitudes with the results of the theoretical computation of the thermal regime for the surface in the approximation of the homogeneous model, with the dependence of thermal conductivity and of specific heat on the temperature taken into consideration [11], results in values for the parameter γ of

$$\gamma_1(300°K) = 1000 \text{ cal}^{-1}\text{-cm}^2\text{-sec}^{1/2}\text{-degree},$$

$$\gamma_2(300°K) = 800 \text{ cal}^{-1}\text{-cm}^2\text{-sec}^{1/2}\text{-degree}$$

respectively, for eclipse and for lunation.

The eclipse values of γ are for the uppermost layer, while the lunation values are for a layer ten times thicker. The closeness of the γ values for the eclipse and lunation processes also favors the approximate homogeneity of the properties in depth.

3. The Parameter $\delta = l_e/l_T$

The effective thickness of the layer under study characterizes the depth of penetration of the electrical wave $l_e = l/\varkappa_v$. It is obvious that the deeper the radiating layer, l_e, as compared with the depth to which the heat wave, l_T, penetrates, the smaller the amplitude of the variation in intensity. The spectrum $\bar{M}(\lambda)$, therefore, characterizes the magnitude of the ratio $\delta = l_e/l_T$. A comparison of the experimental spectrum, $\bar{M}(\lambda)$, with the corresponding theoretical relationship, $\bar{M}_{th}(\lambda)$, obtained through Eq. (22), provides a value of $\delta \simeq 2.3\ \lambda$. The spectrum of magnitude $l_e = 2.3\ l_T\lambda$, points to the dielectrical nature of the material of the upper mantle of the moon just as in the case of the model for the first approximation. It is highly probable that this dielectric can be rocks analogous to terrestrial rocks; that is, silicates. This immediately yields a specific heat value of $c(300) = 0.19$ cal-gram^{-1}-degree^{-1} for all silicates when $T = 300°K$ (accurate to within 10%).

4. Density of the Material of the Surface Layer of the Moon

Eq. (31), cited above, established the factual link between the permittivity of the material and its density. Therefore, all possible methods of measuring ε that are described in what follows in section VIII.6 will provide /1303 the density of the material of the upper mantle. There are data pointing to some minor inhomogeneity in the dielectrical properties of the material in depth in the upper layer of the order of several centimeters. This does not contradict the assertion made above that the spectra of amplitude and phase lag correspond to a homogeneous model. A minor inhomogeneity such that the properties of the material change but slightly with depth, and do so smoothly (by a factor of 1.2 to 1.3 in terms of the density) have little effect on the nature of these spectra, as computations show. In this case, their change falls within the limits of accuracy for the measurements.

If the inhomogeneity is to be detected, those parameters of the radiation must be found that are sensitive to the inhomogeneity. These parameters are the reflection coefficient for radio waves, polarization of the radiation, and the value of the eclipse and night temperature of the surface. An increase in the reflection coefficient in the band of wavelengths between 15 and 30 centimeters (see Figure 25), can indicate a real frequency dependence for the permittivity of the material, or the existence of inhomogeneity in the dielectrical properties according to depth. The first of these assumptions is not valid because increase in ε with the wavelength, according to the Kramers-Kronig theorem, inevitably would result in an increase in the losses in this band of wavelengths, and this would be reflected in the $\bar{M}(\lambda)$ spectrum. This has not yet been observed. The second, apparently, is what takes place.

As pointed out in section IV.3 of this survey, the computation for the reflection coefficient for an exponential change in density with depth revealed that the wavelength, λ, near which the change in the reflection coefficient occurs is linked with the nature of the extent of the layer, y_0, by the relationship

$$20\ y_0 = \lambda_1.$$

By experiment (see Figure 25), $\lambda_1 \simeq 30$ centimeters, so $y_0 \simeq 1.5$ centimeters. The full extent of the inhomogeneous layer is $d_1 \simeq 3$ to 4 centimeters. The

following data satisfy the observed spectrum $R(\lambda)$ in the band 3 cm $\leq \lambda \leq$ 100 cm [35]

$$\rho_1 = (0.6 \text{ to } 0.7) \text{ gram-cm}^{-3},\ \rho_2/\rho_1 = 1.3 - 1.5,\ y_0 = 1.5 \text{ cm}.$$

Measurements of γ in terms of the surface temperatures during eclipse and lunation result in this same degree of inhomogeneity. The difference between γ_1 and γ_2 also indicates the slight increase that takes place in the density with depth. A slight increase in the density of the material with depth also was obtained from the measurements made as part of the Surveyor VII program. Reference [121] points out that a value of $\rho_1 \simeq 1$ gram-cm^{-3} was obtained for the density of the surface material, and that it then increased to $\rho_2 \simeq 1.5$ gram-cm^{-3} in the upper five centimeters of the depth.

It has been possible to investigate the properties of the deeper layers of the moon because of the anomaly of the spectrum of the constant component of the integrated radiofrequency radiation obtained by using the accurate "artificial mood" method. As was pointed out in section III.2 of this survey, the fact that the constant component practically ceases to increase at $\lambda \geq 25$ centimeters indicates a compacting of the material at a depth corresponding to a depth of penetration of wavelengths of 25 to 30 centimeters; that is, the spectrum of the constant component makes it possible to estimate the thickness of the porous layer. Figure 10 shows the theoretical curves constructed through Eq. (23). Experimental points, taken from Figure 21, are plotted in Figure 10 for purposes of comparison. As will be seen, good concordance of theoretical and experimental results can be obtained in the case of thickness of the porous layer of

$$d_2 = 400 \pm 100 \text{ cm} \qquad /1304$$

with density $\rho_2 = 1$ gram-cm^{-3}, and density of the heat flow of

$$q = (0.72 \pm 0.08) \cdot 10^{-6} \text{ cal-cm}^{-2}\text{-sec}^{-1}.$$

The spectrum of the reflection coefficient for radio waves also points to a considerable compacting of the material at a depth of the order of several meters. The increase in the reflection coefficient at wavelengths $\lambda >$ 10 meters [104], apparently points to the fact that the reflection of these waves occurs from denser rocks.

Figure 14 shows the theoretical spectra of the reflection coefficient, computed for the following values for the parameters:

$$y_0 = 1.5 \text{ cm}; \ \rho_1 = 0.7 \text{ gram-cm}^{-3}; \ \rho_2 = 1 \text{ gram-cm}^{-3};$$

$$\rho_3 = 2.5 \text{ gram-cm}^{-3}; \ d_2 = 100, 200, 300 \text{ cm}.$$

Experimental points taken from Figure 25 are plotted in Figure 14 for purposes of comparison. As will be seen, the surface layer model considered for the ρ_1, ρ_2, ρ_3 values indicated describes the observed spectrum of the reflection coefficient quite well. The following value is obtained for the thickness of the porous layer

$$d_2 = 200 \pm 100 \text{ cm}.$$

Radio astronomy measurements provide the magnitude

$$d_2 = 400 \pm 100 \text{ cm}.$$

The latter is apparently the more reliable of the two. Actually, the information on the magnitude of d_2 in the spectrum of the reflection coefficient is derived primarily from three measurements at wavelengths $\lambda > 10$ meters, and the accuracy of these measurements is not very good. Additional radar data in the meter and decimeter band of wavelengths obviously are needed to obtain d_2 from the $R(\lambda)$ spectrum with confidence.

5. Thermal Conductivity, k, and Depth of Penetration of Heat Wave l_T

Using the values $\gamma_1(300)$, $\gamma_2(300)$, ρ_1, ρ_2, and $c(300)$, obtained above, we find that the thermal conductivity of the material of the porous surface is $k_1(300) = (7 \pm 3) \cdot 10^{-6}$ cal-cm^{-1}-sec^{-1}-degree^{-1}, and that the thermal conductivity of the porous layer is $k_2(300) = (9 \pm 4) \cdot 10^{-6}$ cal-cm^{-1}-sec^{-1}-degree^{-1}. The thermal conductivity values cited here for k_1 and k_2 are for temperature $T = 300°K$.

In accordance with Eq. (6), the depth of penetration of the heat wave equals

$$l_T = \left(\frac{2k}{\rho c \Omega}\right)^{1/2} \simeq 7.5 \text{ cm}.$$

6. Electromagnetic Properties of the Material: Depth of Penetration of the Electrical Wave l_e; Permittivity ε; and the Specific Tangent of the Angle of Loss $\tan(\Delta/\rho)$

Already obtained above is the fact that $l_e/l_T = 2.3\ \lambda$, and that $l_T \simeq 7.5$ centimeters. Then in $l_e \simeq 17\ \lambda$.

As has already been mentioned, several methods have been proposed for finding the permittivity, ε, of the material of the upper mantle of the moon, such as finding ε through the polarization of the natural radiation [43-48, 102], from the distribution of brightness temperature over the disk [37, 89, 101], from a determination of the phase lag in the radiofrequency radiation from sections of the disk located at different longitudes along the equator of the moon as compared with the phase of heating of these sections [122], and from direct, local, measurements of the reflection [104-108]. All of these methods are based on the fact that the surface of the moon is quite smooth, so the reflection coefficient is correct for the Fresnel formula.

The polarization method for finding ε was used in references [43, 109, 123-125]. These measurements provide a magnitude of $\varepsilon_1 \simeq 2$ for the permittivity of the material of the surface, and a magnitude of $\varepsilon_2 \simeq 2.5$ for the permittivity of the material of the solid porous layer. /1305

The magnitudes $\rho_1 = 0.75$ gram-cm^{-3} and $\rho_2 = 1$ gram-cm^{-3} were obtained for densities ρ_1 and ρ_2 using the ε values found through Eqs. (31) and (32), and these magnitudes coincide with the values for these same magnitudes obtained above from the spectra of the reflection coefficient and the constant component of the radiofrequency radiation.

A comparison between the spectrum of the change in intensity during lunar eclipse and theory provides the specific tangent of the angle of loss $b_1 = \tan \Delta_1/\rho_1$ for the first few centimeters of the layer (see section III.3 of this survey).

This magnitude for the centimeter band is equal to

$$b_1 = (9 \pm 3) \cdot 10^{-3}.$$

Turning our attention to the values for c, γ_2, and ε_2, obtained from the lunation measurements, we have $b_2 = (8 \pm 2) \cdot 10^{-3}$.

7. Chemical Composition of the Lunar Material

The method described in section VII of this survey was used to find the chemical composition of the moon material. Using the curves in Figure 26, and

the value $b = (9 \pm 3) \cdot 10^{-3}$, it is easy to find that the upper mantle of the moon material has the following mean hemispheric chemical composition

SiO_2 — 57 ± 3%, Al_2O_3 — 16 ± 1%, Fe_2O_3 — 1 ± 2%,
FeO — 5 ± 1%, CaO — 5,5 ± 2,5%, MgO — 3,5 ± 2%,
Na_2O — 4 ± 0,5%, K_2O — 3 ± 1%, TiO_2 — 1 ± 0,5%.

Table 2 compares the results of chemical analysis obtained using this method with the results of analysis of data obtained by the Surveyors [119] (the composition is expressed in percentage of atom content).

TABLE 2.

Element	Surveyor-V	Surveyor-VI	Surveyor-VII	Radio astronomy
O	58±5	57±5	58±5	62±4
Si	18,5±3	22±4	18±4	20±1
Al	6,5±2	6,5±2	9±3	7±0,5
Mg	3±3	3±3	4±3	2±1
Fe, Ca	13±3	5±2, 6±2	2±1, 6±1	2±0,5, 2±1
K	—	—	—	1,5±0,5
Na	2	2	3	1,5±0,5

Commas represent decimal points.

The concordance is very good, as will be seen from the table. (The data obtained by the Surveyors included the K concentration, and this must be borne in mind when comparing the Ca values).

It is interesting to compare these results with the results of the analysis made of the material obtained by the astronauts of Apollo 11. The following mean chemical composition of the lunar material has been cited in [63]

SiO_2—41%; CaO—10.5%; MgO—8%; FeO—18%; Al_2O_3—11.3%;
N_2O—0,6%; Ka_2O—0.2%; TiO_2—10%.

There is a very significant difference between the two sets of data, with the latter showing much greater percentages of oxides of iron, magnesium, and

calcium, as well as orders of magnitude more titanium dioxide. One cannot help but note the significantly smaller percentages of oxides of potassium and sodium. The authors of [63] explain these anamolies by the evaporation of fusible oxides in the process that has evolved during the moon's thermal history. /1306

8. The Microstructure of the Material of the Upper Mantle of the Moon

As has been indicated above [13], if the material of the moon is opaque at infrared wavelengths, the radiative transfer of radiation through the pores will be $k_{rn}/k_0 = 0.25$, whereas if it is penetrable $kr/k_0 = 0.4$. Taking $k = k_r + k_0 = (9 \pm 3) \cdot 10^{-6}$ cal-cm^{-1}-sec^{-1}-degree^{-1}, we obtain $k_{rn} = (1.5\text{-}2.5) \cdot 10^{-6}$ cal-cm^{-1}-deg^{-1}-sec^{-1}, or $k_r + (2.0\text{-}3.5) \cdot 10^{-6}$ cal-cm^{-1}-deg-sec^{-1}.

Solving Eq. (7) for k_{rn}, we find that the effective size of the pores is 170 to 350 microns. Since material porosity is close to 50%, pore size should be approximately equal to particle size. If it is considered that the material is penetrable at infrared wavelengths, then, in accordance with Eq. (8), and in accordance with the k_r value cited, a = 6 to 12, and l_e = 6 to 12 λ for infrared wavelengths. As we have seen, l_e = 17 λ for wavelengths longer than 1000 microns. It seems to us that it is more probable that the material is penetrable at infrared wavelengths. Then, in order for the transport of heat through the pores to be slight, the latter, and consequently the particles of the material too, should be many times smaller than the mean free path of the infrared quantum, equal to l_e = 60 to 120 microns. This can be so, apparently, for particles from tens to several tens of microns in size [13].

9. Homogeneity of Surface Properties

The results obtained above, with the exception of the data for γ, are averaged for the entire hemisphere of the moon. Therefore, it is only natural to question the degree to which they correspond to local values. According to investigations conducted at infrared wavelengths, the disk thermal properties, with the exception of the bottoms of the lunar craters, change very little, no more than from 20 to 25% [126]. These changes are within the practical limits of accuracy for the measurements. Observed as well was a high degree of homogeneity of radiofrequency radiation characteristics for the disk, characteristics such as $\overline{M}(\lambda)$ and $\overline{\xi}_1$, when small areas, ranging from tens to hundreds of kilometers, were averaged [87-91, 126].

One can, therefore, discuss the existence of radiometric homogeneity, analogous to the known photometric homogeneity [127] associated with the homogeneity of the characteristics of reflected light. Radiometric homogeneity implies homogeneity in the distribution of the electrical properties of the material on the moon's surface through a layer at least 10 centimeters thick. In particular, it appears that the material on the surfaces of the maria and continents is practically identical [126]. Clearly, it does not correspond to the characteristics of radiation based on the hypothesis that the upper rock of the continents is granite, that of the maria, basalt.

More precise measurements of the distribution of radiofrequency radiation from the disk of the moon at a wavelength of $\lambda = 8$ millimeters [64] found some difference in the properties, and lead to the conclusion that the density of the material of the maria evidently is somewhat greater than is that of the material of the continents.

The characteristics obtained are real properties of the material at each site, because of the great homogeneity along the horizontal of the properties of the upper mantle. The high degree of homogeneity of properties is confirmed by the results obtained from direct investigations made of the moon. However, the investigation made of the chemical composition as part of the Surveyor program established the fact that the maria contain 2 to 3 times the ion oxides /1308 found on the continents.

10. General Model of the Structure of the Upper Layer of the Moon

Everything discussed in the foregoing leads to the statement that the upper mantle of the moon can be described most completely by a four-layer model. True, in reality the density changes quite smoothly from layer to layer, and this change is such that this separation into layers is introduced somewhat conditionally in order to simplify the picture. Table 3 lists the properties of these layers.

TABLE 3

Name of layer	Depth of layer, d (cm)	Density, ρ (gram-cm^{-3})	Porosity, p (%)	Thermal conductivity, $k(300)\cdot10^6$ cal/cm-sec-degree	Specific heat $c(300)$ cal/gram-degree	Thermal inertia, γ cm^2-sec$^{1/2}$ /cal-degree	Depth of penetration of heat wave l_T (cm)	Density of heat flow $q\cdot10^6$ cal/cm^2-sec	Permittivity, ε	Specific tangent of the angle of loss tan Δ/ρ	Depth of penetration of electromagnetic waves l_ε (cm)	
									At centimeter wavelengths			
Porous surface	0—4	0,7±0.2	80	7±3	0.19	1000	7,5	0,7—0,8	2±0,2	9±3	15—17λ	
Porous layer	4—400	$1^{+0,2}_{-0,1}$	60	9±3	0,19	800	7,5	0,7—0,8	2,5±0,2	8±2	15—17λ	
Transition layer	400—600	1,5—2	30	10^3	0,19				3,5			
Rocks	Over 600	2,5—3	0—10	$5\cdot10^3$	0,19				5—6			

71307

IX. Conclusion

As this review has pointed out, investigation of natural thermal radiation from the moon results in the obtaining of quite complete data concerning the temperature regime on the surface of the moon, on its physical conditions, and on the structure of the material. The objectivity of the data obtained is confirmed by the results of direct investigation of the moon. This is the basis for the confident belief that the methods developed for analyzing and interpreting the data can be used successfully to investigate some of the other planets, Mars, for example, the physical conditions on which are close to those on the moon.

The authors express their thanks to V. D. Krotikov for valuable discussions concerning the survey.

REFERENCES

1. Pettit, E. and Nicolson, S. B., Astrophys. J., Vol. 72, 1930, p. 102.
2. Dicke, R. H. and Beringer, R., Astrophys. J., Vol. 103, 1946, p. 735.
3. Krotikov, V. D. and Troitskiy, V. S., UFN, Vol. 81, 1963, p. 589.
4. Troitskiy, V. S., J. Res. NBS, Vol. 69D, No. 12, 1965, p. 1585.
5. Horald, W., Solar Syst. Radio Astron., Atheus. Ionosph. Inst. Nat. Observ., 1965, p. 295.
6. Troitskiy, V. S., Izv. vysh. uch. zav.-Radiofizika, Vol. 10, No. 9-10, 1967, p. 1266.
7. Troitskiy, V. S., Phil. Trans. Royal Soc. London, Vol. A264, 1969, p. 145.
8. Wesselink, J. C., Bull. Astron. Inst. Neth., Vol. 10, 1948, p. 351.
9. Jaeger, J. G., Austr. J. Phys., Vol. 6, 1953, p. 10.
10. Krotikov, V. D. and Shchuko, O. B., Astron. zh., Vol. 40, 1963, p. 297.
11. Troitskiy, V. S., Burov, A. B. and Alyoshina, T. N., Icarus, Vol. 8, 1968, p. 423.
12. Troitskiy, V. S., Astron. zh., Vol. 31, 1954, p. 51.
13. Troitskiy, V. S., Nature, Vol. 213, 1967, p. 688; Troitskiy, V. S., Izv. vysh. uch. zav.-Radiofizika, Vol. 10, No. 8, 1967, p. 1051.
14. Ingrao, H. C., Young, A. T. and Linsky, J. L., Harv. Coll. Observ. Rep., No. 6, 1965.
15. Muncey, R. W., Nature, Vol. 181, 1958, p. 1458.
16. Troitskiy, V. S., Astron. zh., Vol. 39, 1962, p. 73.
17. Alekseyev, V. A., Drobova, L. V. and Krotikov, V. D., Astron. zh., Vol. 45, 1968, p. 1101.
18. Welch, W. J., Thornton, D. D. and Winter, S., J. Geophys. Res., Vol. 70, 1965, p. 2793.
19. Troitskiy, V. S., Astron. zh., Vol. 42, 1965, p. 1296.
20. Pettit, E., Astrophys. J., Vol. 91, 1940, p. 408.
21. Shorthill, R. W. and Saary, J. M., Science, Vol. 150, 1965, p. 210.
22. Gear, A. E. and Bastin, J. A., Nature, Vol. 196, 1962, p. 1305.
23. Buhl, D., Ph. D. Thesis, University of California, 1967.
24. Hagfors, T., J. Geophys. Res., Vol. 69, 1964, p. 3779.
25. Smith. B. G., J. Geophys. Res., Vol. 72, 1967, p. 4059.
26. Ingrao, H. C., Yong, A. T. and Linsky, J. L., The Nature of the Lunar Surface, The Johns Hopkins Press, Baltimore, 1966, p. 185.

27. Hopfield, J. J., Science, Vol. 151, 1966, p. 1380.

28. Roelof, E. C., Icarus, Vol. 8, 1968, p. 138.

29. Tikhonova, T. B. and Troitskiy, V. S., Astron. zh., Vol. 46, 1969, p. 159.

30. Brekhovshikh, A. M., Volny v sloistykh sredakh, [Waves in Stratified Media], AN SSSR, Moscow, 1957.

31. Krotikov, V. D., Izv. vysh. uch. zav.-Radiofizika, Vol. 6, No. 5, 1963, p. 889.

32. Troitskiy, V. S., Izv. vysh. uch. zav.-Radiofizika, No. 5, No. 3, 1962, p. 602.

33. Krotikov, V. D. and Troitskiy, V. S., Astron. zh., Vol. 40, 1963, p. 1076.

34. Krotikov, V. D. and Troitskiy, V. S., Izv. vysh. uch. zav.-Radiofizika, Vol. 6, No. 3, 1963, p. 633.

35. Matveyev, Yu. G., Suchkin, G. L. and Troitskiy, V. S., Astron. zh., Vol. 42, 1965, p. 810.

36. Krotikov, V. D. and Troitskiy, V. S., Astron. zh., Vol. 39, 1962. p. 1089.

37. Alekseyev, V. A., Aleshina, T. N., Krotikov, V. D. and Troitskiy, V. S., Astron. zh., Vol. 44, 1967, p. 1070.

38. Bogdanov, A. A., Brusin, I. Ya., Kagorlitskiy, M. S. and Tikhonova, T. V., Izv. vysh. ush. zav.-Radiofizika, Vol. 11, No. 6, 1968, p. 801.

39. Tikhonova, T. V. and Troitskiy, V. S., Astron. zh., Vol. 46, 1969, p. 1324.

40. Bondar', L. N., Strezhneva, K. M. and Troitskiy, V. S., Fizika Zemli, [Physics of the World], (in print).

41. Alekseyev, V. A. and Krotikov, V. D., Izv. vysh. uch. zav.-Radiofizika, Vol. 11, No. 8, 1968, p. 1133.

42. Hagfors, T. and Moriella, J., Radio Science, Vol. 69D, 1965, p. 1614.

43. Soboleva, N. S., Astron. zh., Vol. 39, 1962, p. 1124.

44. Losovskiy, B. Ya., Astron. zh., Vol. 44, 1967, p. 416.

45. Soboleva, N. S., Izv. GAO, Issue 6, 1967, p. 205.

46. Alekseyev, V. A., Aleshina, T. N. and Krotikov, V. D., Izv. vysh. uch. zav.-Radiofizika, Vol. 10, No. 5, 1967, p. 604.

47. Alekseyev, V. A. and Krotikov, V. D., Izv. vysh. uch. zav.-Radiofizika, Vol. 12, No. 1, 1969, p. 5.

48. Alekseyev, V. A., Aleshina, T. N., Krotikov, V. D. and Mol'kova, L. A., Simpozium po fizike Luny i planet, [Symposium on the Physics of the Moon and the Planets], Kiev, 1968.

49. Winter, D., Boeing Sci. Res. Lab. Doc., DI-82-0717, 1968.

50. Murray, B. C. and Wildey, R. L., Astrophys. J., Vol. 139, 1964, p. 734.

51. Low, F. J., Astrophys. J., Vol. 142, 1965, p. 806.

52. Shorthill, R. W. and Saary, J. M., Boeing Sci. Res. Lab. Doc., DI-82-0778, 1969.

53. Saary, J. M. and Shorthill, R. W., Icarus, Vol. 2, 1963, p. 115.

54. Buettner, K. J. K., Planet. Space Sci., Vol. 11, 1963, p. 135.

55. Bastin, J. A., Nature, Vol. 207, 1965, p. 1381.

56. Messger, P. G. and Strassl. H., Planet. Space Sci., Vol. 1, 1959, p. 213.

57. Krotikov, V. D., Porfir'yev, V. A. and Troitskiy, V. S., Izv. vysh. uch. zav.-Radiofizika, Vol. 4, No. 6, 1961, p. 1004.

58. Tseytlin, N. M., Izv. vysh. uch. zav.-Radiofizika, Vol. 6, No. 6, 1963, p. 1265.

59. Tikhonova, T. V., Izv. vysh. uch. zav.-Radiofizika, Vol. 12, No. 8, 1969, p. 1121.

60. Bondar', L. N., Zelinskaya, M. R., Porfir'yev, V. A. and Strezhneva, K. M., Izv. vysh. uch. zav.-Radiofizika, Vol. 5, No. 4., 1962, p. 802.

61. Semenov, B. N., Kamenskaya, S. A., Troitskiy, V. S. and Plechkov, V. M., Izv. vysh. uch. zav.-Radiofizika, Vol. 5, No. 5, 1962, p. 882.

62. Krotikov, V. D., Izv. vysh. uch. zav.-Radiofizika, Vol. 5, No. 3, 1962, p. 604.

63. Science, Vol. 165, No. 3899, 1969, p. 1211.

64. Krotikov, V. D. and Porfir'yev, V. A., Izv. vysh. uch. zav.-Radiofizika, Vol. 6, No. 2, 1963, p. 242.

65. Krotikov, V. D., Izv. vysh. uch. zav.-Radiofizika, Vol. 6, No. 6, 1963. p. 1087.

66. Dmitrenko, D. A., Kamenskaya, S. A. and Rakhlin, V. L., Izv. vysh. uch. zav.-Radiofizika, Vol. 7, No. 3, 1964, p. 555.

67. Zakharov, A. V., Krotikov, V. D., Troitskiy, V. S. and Tseytlin, N. M., Izv. vysh. uch. zav.-Radiofizika, Vol. 7, No. 3, 1964, p. 553.

68. Krotikov, V. D., Troitskiy, V. S. and Tseytlin, N. M., Astron. zh., Vol. 41, No. 5, 1964, p. 951.

69. Alekseyev, B. A., Krotikov, V. D., Matveyev, Yu.G., Mikhaylova, N. B., Porfir'yev, B. A., Ryazanov, V. P., Sergeyeva, A. I., Strezhneva, K. M., Troitskiy, V. S. and Shmulevich, S. A., Izv. vysh. uch. zav.-Radiofizika, Vol. 9, No. 5, 1966, p. 1030.

70. Plechkov, V. M., Astron. zh., Vol. 44, No. 1, 1967, p. 154.

71. Alekseyev, V. A., Bondar', L. N., Kamenskaya, S. A., Krotikov, V. D., Matveyev, Yu. G., Strezhneva, K. M. and Troitskiy, V. S., Astron. zh., Vol. 44, No. 3, 1967, p. 593.

72. Piddington, J. H. and Minnet, H. G., Austr. J. Sci. Res., Vol. 2A, 1949, p. 643.

73. Hagen, J. P., NRL Report, No. 3504, 1949.

74. Piddington, J. H. and Minnet, H. G., Austr. J. Sci. Res., Vol. 4A, 1951, p. 459.

75. Troitskiy, V. S. and Zelinskaya, M. R., Astron. zh., Vol. 32, No. 6, 1955, p. 550.

76. Solomonovich, A. Ye., Astron. zh., Vol. 35, No. 1, 1958, p. 129.

77. Zelinskaya, M. R., Troitskiy, V. S. and Fedoseyev, L. I., Astron. zh., Vol. 36, No. 4, 1959, p. 643.

78. Zelinskaya, M. R., Troitskiy, V. S.,and Fedoseyev, L. I., Izv. vysh. uch. zav.-Radiofizika, Vol. 2, No. 3, 1959, p. 506.

79. Kislyakov, A. G., Izv. vysh. uch. zav.-Radiofizika, Vol. 4, No. 3, 1961, p. 433.

80. Strezhneva, K. M. and Troitskiy, V. S., Izv. vysh. uch. zav.-Radiofizika, Vol. 4, No. 4, 1961, p. 600.

81. Medd, W. J. and Broten, N. W., Planet Space Sci., Vol. 5, 1961, p. 307.

82. Kislyakov, A. G., Astron. zh., Vol. 38, No. 3, 1961, p. 561.

83. Troitskiy, V. S., Krotikov, V. D. and Tseytlin, N. M., Astron. zh., Vol. 44, No. 2, 1967, p. 413.

84. Naumov, A. I., Izv. vysh. uch. zav.-Radiofizika, Vol. 6, No. 4, 1963, p. 847.

85. Fedoseyev, L. I., Izv. vysh. uch. zav.-Radiofizika, Vol. 6, No. 4, 1963, p. 655.

86. Razin, V. A. and Fedorov, V. T., Izv. vysh. uch. zav.-Radiofizika, Vol. 6, No. 5, 1963, p. 1052.

87. Koshchenko, B. N., Kuz'min, A. D. and Solomonovich, A. Ye., Izv. vysh. uch. zav.-Radiofizika, Vol. 4, No. 4, 1961, p. 596.

88. Solomonovich, A. Ye. and Koshchenko, V. N., Izv. vysh. uch. zav.-Radiofizika, Vol. 4, No. 4, 1961, p. 591.

89. Solomonovich, A. Ye. and Losovskiy, B. Ya., Astron. zh., Vol. 39, No. 6, 1962, p. 1074.

90. Solomonovich, A. Ye., Astron. zh., Vol. 39, No. 1, 1962, p. 79.

91. Kislyakov, A. G. and Solomonovich, A. Ye., Izv. vysh. uch. zav.-Radiofizika, Vol. 6, No. 3, 1963, p. 431.

92. Solomonovich, A.Ye., Proc. Roy. Soc., Vol. 296, 1967, p. 354.

93. Mayer, C. H., McCullough, R. M. and Sloanaker, R. M., The Solar System, Vol. 3, Univ. Chicago, 1961.

94. Gibson, J. E., Astrophys. J., Vol. 133, 1961, p. 1072.

95. Sinton, W. M., Astrophys. J., Vol. 123, No. 2, 1956, p. 325.

96. Shorthill, R. W., Borough, H. C. and Canley, J. M., Publ. Astron. Soc. Poc., Vol. 72, No. 429, 1960, p. 481.

97. Castelli, J. P., Ferioli, C. P. and Aarons, J., Astronom. J., Vol. 65, No. 9, 1960, p. 485.

98. Saary, J. M. and Shorthill, R. W., Boeing Sci. Res. Lab., July, 1962.

99. Kamenskaya, S. A., Kislyakov, A. G., Krotikov, V. D., Plechkov, V. M., Naumov, A. I., Nikonov, V. N., Porfir'yev, V. A., Strezhneva, K. M., Troitskiy, V. S., Fedoseyev, L. I., Lubyako, L. V. and Sorokina, E. P., Izv. vysh. uch. zav.-Radiofizika, Vol. 8, No. 2, 1965, p. 219.

100. Plechkov, V. M., Astron. zh., Vol. 43, No. 1, 1966, p. 172.

101. Koshchenko, V. N., Kuz'min, A. D. and Solomonovich, A. Ye., Izv. vysh. uch. zav.-Radiofizika, Vol. 4, No. 4, 1961, p. 596.

102. Troitskiy, V. S. and Tseytlin, N. M., Izv. vysh. uch. zav.-Radiofizika, Vol. 3, No. 6, 1960, p. 1127.

103. Evans, J. V., Physics and Astronomy of the Moon, Acad. Press, N. Y., London, 1962, p. 429.

104. Evans, J. V., J. Res. Nat. Bur. Stand., Vol. 69D, No. 12, 1965, p. 1637.

105. Giraund, A., J. Res. Nat. Bur. Standards, Vol. 69D, No. 12, 1965, p. 1677.

106. Davis, J. R., Rahlfs, D. C., Skaggs, G. A. and Joss, J. W., J. Res. Nat. Bur. Standards, Vol. 69D, No. 12, 1965, p. 1659.

107. Evans, J. V. and Hagfors, T., J. Geophys. Res., Vol. 71, No. 20, 1966, p. 4871.

108. Khegfors, T., Simpozium po fizike Luny i planet, [Symposium on the Physics of the Moon and the Planets], Kiev, 1968.

109. Davies, R. D. and Gardner, F. F., Aust. J., Vol. 19, No. 16, 1966, p. 823.

110. Barabashov, N. P. and Chekirda, A. T., Astron. zh., Vol. 3, 1960, p. 827.

111. Hapke, B. and Van Horn, H., CRSR 139, Cornell University, Ithaca, New York, February 1963.

112. Hapke, B., Astron. J., Vol. 71, 1966, p. 333.

113. Lyot, B., Ann. de J'Obs. de Paris, Sect. de Medon, Vol. 8, 1929.

114. Dollfus, A., Ann. Astrophys., Vol. 19, 1956, No. 2.

115. Krotikov, V. D., Izv. vysh. uch. zav.-Radiofizika, Vol. 5, No. 6, 1962, p. 1057.

116. Fensler, W. E., Knott, E. F., Olte, A. and Siegel, K. M., IAU Symposium, Acad. Press, N. Y., London, 1962, p. 14.

117. Olte, A. and Siegel, K. M., Astrophys. J., Vol. 133, 1961. p. 706.

118. Betekhtin, A. G., Kurs mineralogii, [A Course in Minerology], GNT Press, Moscow, 1956.

119. Troitskiy, V. S., Bondar', L. N., Zelinskaya, M. R. and Strezhneva, K. M., Astron. vestnik, Vol. 3, No. 4, 1969.

120. Krupenno, N. N., Dissertation, IKI AN SSSR, 1969.

121. Jaffe, L., Science, Vol. 164, 1969, p. 1514.

122. Troitskiy, V. S., Astron. zh., Vol. 38, 1961. p. 1001.

123. Heiles, G. E. and Drake, F. D., Icarus, Vol. 2, 1963, p. 281.

124. Gol'nev, Soboleva, N. S., Pros. Astro. Obs. Pulkova, Vol. 13, 1964, p. 83.

125. Baars, J. W., Mezger, P. G., Savin, N. and Wendker, H., Astr. J., Vol. 70, 1965, p. 132.

126. Troitskiy, V. S., Astron. zh., Vol. 59, 1964, p. 724.

127. Barabashov, N. P., Yezerskaya, V. A., Yezerskiy, V. I. and Ishutina, T. I., Izv. kom. po fiz. planet, No. 1, 1959, p. 67.

128. Campbell, J. J., Ulrichs, J. and Hapke, B., CRSR, Cornell University, Ithaca, New York, February 1969.

129. Linsky, J. L., Icarus, Vol. 5, No. 6, 1966, p. 606.

130. Stimpson, L. D. and Lucas, J. W., Report JPR, No. NAS 7-100, 1968.

131. Fedoseyev, L. I., Lubyako, L. V. and Kukin, L. M., Izv. vysh. uch. zav.-Radiofizika, Vol. 11, No. 6, 1968, p. 807.

132. Kislyakov, A. G. and Plechkov, V. M., Izv. vysh. uch. zav.-Radiofizika, Vol. 7, No. 1, 1964, p. 46.

133. Waak, J. A., Astron. J., Vol. 66, 1961, p. 298.

134. Baldwin, J. E., Month Not. Roy. Astron. Soc., Vol. 122, 1961, p. 513.

The Radiophysical Scientific Research
Institute of Gor'kii University

Went to print
3 December 1969

Translated for the National Aeronautics and Space Administration
under contract No. NASw-2038 by Translation Consultants, Ltd.,
944 South Wakefield Street, Arlington, Virginia 22204